Integrating Genome-Scale and Pharmacokinetic Models towards Precision Medicine and the Prediction of Tetrahydrocannabinol and Ethanol Metabolism

by

Leo Zhengyue Zhu

A thesis submitted in conformity with the requirements
for the degree of Master of Applied Science

Graduate Department of Chemical Engineering and Applied Chemistry
University of Toronto

Integrating Genome-Scale and Pharmacokinetic Models towards Precision Medicine and the Prediction of Tetrahydrocannabinol and Ethanol Metabolism

Leo Zhengyue Zhu
Master of Applied Science
Graduate Department of Chemical Engineering and Applied Chemistry
University of Toronto
2020

Abstract

Cannabis and Ethanol are two of the most frequently used recreational substances in the world and many health policies are devoted towards ensuring their safe consumption. In this thesis, the metabolism of tetrahydrocannabinol (THC) and ethanol are modelled to gain further understanding of how these compounds affect the body. First, a physiologically-based pharmacokinetic (PBPK) model was developed to characterize how individuals with different genotypes eliminate THC as well as its effect (in conjunction with ethanol) on driving. Then, a previously developed PBPK model of ethanol metabolism was combined with a whole-body genome-scale model (GEM) to better predict how genetic variations and diseases could affect ethanol metabolism and exposure to the carcinogenic metabolite, acetaldehyde. By gap-filling enzyme-specific PBPK models with general metabolic fluxes from GEMs, we can predict the impact of inter-individual variations on drug metabolism and steer the modelling field towards precision medicine and the development of a “virtual twin”.

Acknowledgments

I would like to express my utmost gratitude to my supervisor, Professor Radhakrishnan Mahadevan, for his valuable guidance throughout every aspect of my graduate career. His advice and mentorship was crucial in helping me adjust to the drastically different lifestyle of graduate school, and his trust in allowing me to pursue collaborations and to advise thesis students allowed me to gain a lot of experience that would be valuable in my future career.

This projects would not have been possible without the assistance and guidance from my collaborators at the Center for Addiction and Mental Health (Dr. Patricia DiCiano, Dr. Bruna Brands) as well as the National University of Ireland at Galway (Professor Ines Thiele). I would also like to thank Professor Alison McGuigan and Professor Bradley Saville for their feedback during my oral examination.

Furthermore, I would like to acknowledge Marios Mejdani, Kaushik Raj, Christian Euler and my colleagues at the Laboratory for Metabolic Systems Engineering, BioZone, my thesis students (Timothy Liu and William Pei), the NSERC CREATE M3 Scholarship Program, and the MacLean Foundation Scholarship Program for all of their help over the last two years.

Lastly, a big thank you is owed to my family, friends, and mentors for the support that they gave me throughout this time. Special shoutout to MCAT, Grace, Dallas, Kaiwen, Alan, Julia, Jenny, Jenny, Lucy, and all of the boys.

Table of Contents

Table of Contents

List of Tables

List of Figures

List of Appendices

List of Abbreviations

ADME	Adsorption, Distribution, Metabolism, and Elimination
PBPK	Physiologically-Based Pharmacokinetic
GEM	Genome-Scale Model
FBA	Flux Balance Analysis
KEGG	Kyoto Encyclopedia of Genes and Genomes
COBRA	Constraint-Based Reconstruction and Analysis
EHMN	Edinburgh Human Metabolic Network
IEM	Inborn Errors of Metabolism
AGORA	Assembly of Gut Organisms through Reconstruction and Analysis
VMH	Virtual Metabolic Human
THC	Tetrahydrocannabinol
CBD	Cannabidiol
CYP2C9	Cytochrome P450 2C9
AUC	Area Under the Curve
ADH	Alcohol Dehydrogenase
ALDH2	Aldehyde Dehydrogenase
DME	Drug Metabolizing Enzyme
SDLP	Standard Deviation of Lateral Position
PK	Pharmacokinetic
MAE	Mean Absolute Error

1 Literature Review

1.1 Pharmacokinetic Modelling

In the drug discovery process, candidates must be tested for safety, efficacy, and a proper dosing regimen must be developed. To determine these factors, models are developed to better understand the absorption, distribution, metabolism, and elimination (ADME) of these various compounds. Through the bottom-up development of models by using pharmacokinetic, pharmacodynamic, physiological, and metabolic data, comprehensive models of the interactions between human metabolism and xenobiotic compounds can be evaluated.

The first Physiologically-Based Pharmacokinetic (PBPK) Model was developed by Teorell in 1937 to gauge the concentrations of metabolites over time in tissues other than blood, but this was too complicated to be used effectively for general predictions [1,2]. Decades later during the 1970s, the increased availability of computational software and analytical solvers allowed for a resurgence of PBPK models [3]. At this time, there were many variations between models as each group would have its own set of model parameters, thus Brown and colleagues established a repository of physiological parameters for various animals and humans for the exclusive purpose of building PBPK models, which continues to be used today [4]. Some of these animal parameters were used in allometric modelling, where predictions are made for humans based on performances in animals due to a lack of information surrounding human distribution [5].
To better predict the distribution of compounds across a variety of human tissues, the PBPK modelling community turned towards using drug properties and tissue composition to create tissue:plasma partition coefficients. This work began with Poulin's correlations that took advantage of the proportion of water, neutral lipids, and phospholipids in tissue as well as the drug's lipophilicity and fraction unbound [6]. In future iterations of this work, adjustments were made for acidic, basic, neutral and zwitterionic compounds [7][8].

By combining the physiological backbone with drug-specific parameters, PBPK models became readily accepted in regulatory affairs and were used to predict drug distribution of tissue-targeted drugs. Specifically, physiological information relating organ weight, organ volume,

cardiac output, organ blood flow, composition, transporters, enzymes, membrane surface areas were combined with drug-related information on membrane permeability, protein binding, tissue:plasma ratio, clearance rates and transport rates to develop PBPK models [9].
These models were initially constructed in open-software platforms such as MATLAB, acsIX, ADAPT 5, MCSIM, or SAAM II, but as the pharmaceutical industry took greater interest in optimizing drug discovery, proprietary closed-software platforms such as Chloe PK, GastroPlus, MEDICI-PK, PK-SIM, and Simcyp began to emerge [9]. The closed-software platforms compiled their own repository of parameters, and included modular graphical user interfaces to facilitate researchers in developing PBPK models. Nevertheless, there is a lack of comprehensive information in this space (especially surrounding human data), and thus this bottom-up approach is often complemented by top-down model parameter fitting with clinical data for gap filling. PBPK models eventually became the industry standard for drug discovery and federal regulation, with the Food and Drug Administration even hosting seminars to discuss its value in dose selection [2,10-12].

Recently, these models have taken an approach towards precision medicine by including more individual-specific parameters and accounting for drug-drug interactions. PBPK modellers envision a future in which patients have an *in-silico* PBPK twin for testing drug cocktails and dosing regimen for safety and efficacy prior to *in-vivo* administrations [13]. Furthermore, genetic differences and disease states can be accounted for in the model to further improve the personalization. At Pfizer, one of the world's leading pharmaceutical companies, PBPK models are used in all aspects of drug discovery, leading to increased efficiency, reduced animal studies, and could potentially replace clinical trials, ultimately increasing the understanding of pharmacokinetics [14]. This discovery process extends to oncological studies, nanoparticle formulations, and can even assess the impact of breastfeeding and placental delivery of drugs [15-17]. With the increase of omics studies in human health, enormous amounts of data related to genomics, transcriptomics, proteomics, and metabolomics can be integrated to the PBPK models to provide further personalization [18].

Furthermore, PBPK models provide value in gauging the effects of phenotype, sex, age, disease, biorhythms on various drugs, especially for fields related to vulnerable populations including pediatrics, geriatrics, and obstetrics [18-20]. Diseased states such as hepatic cirrhosis, renal impairment, or even gastrectomy patients could have their drug exposures assessed virtually prior to administration [19]. However, there is a lack of standardized PBPK model testing, often relying on visual predictive tests, observed/predicted ratios, or root mean square error between the model and its validation data [19]. Models with 2-3 fold differences from clinical data are heralded as a triumph and thus many more advances are necessary to achieve the PBPK dream of a “virtual twin” [21]. Nevertheless, PBPK models today are a standard in the pharmaceutical industry with a wide array of applications in drug-drug interactions, drug metabolism, nanoparticle transport and even modelling special human populations [22]. PBPK predictions span across a broad variety of medical fields, and their continued development can ultimately revolutionize the field of precision medicine [22].

1.2 Genome Scale Modelling

Metabolism is a complex phenomenon which relates to the central dogma of genetics: genes are transcribed to transcripts, which are translated to proteins to carry out functions in the body. Within an organism, a myriad of reactions happen simultaneously, carefully balancing thousands of metabolites to ensure survival.

In 1999, Edwards et al. developed the first genome-scale model (GEM) of *H. influenzae*, identifying and categorizing genes into the functions of central metabolism, alternative carbon sources, amino acid metabolism, purine/pyrimidine metabolism, vitamin/cofactor metabolism, lipid metabolism, and cell wall metabolism [23]. These functions are crucial to the bacteria's survival, and understanding of the essential genes can allow for the identification of drug targets. Edwards then pivoted to create MG1655, the first *E. coli* GEM with the addition of a gene category related to transport mechanisms [24]. Here the Flux Balance Analysis (FBA) technique was developed to gauge the effect of various gene knockouts and used to predict the fluxes through various pathways in the metabolic network reconstruction.

In FBA, the metabolites and reactions in the GEM are represented as a stoichiometry matrix (S), and S is multiplied by a vector of fluxes (v) such that the sum of all of the fluxes in the organism is zero (Sv=0) [25]. These fluxes were subject to various constraints (lower bound, lb; upper bound, ub), and solving the model to maximize an objective function ($f^T v$) allows for insight into the fluxes through individual reactions (See Equation 1.1). While each protein in the reconstruction can be characterized for its kinetic data, doing so is an extremely time consuming process, and it is computationally more efficient to assume a pseudo-equilibrium state in the organism and use the stoichiometric ratios of reactions to further the understanding of metabolism [26]. The rationale behind the pseudo-equilibrium is that the cellular processes occur at a much faster time scale when compared to organism growth, and thus there would be no net change in metabolite concentrations [25].

$$\begin{aligned} &\mathbf{max} \quad \mathbf{f^T v} \\ &\mathbf{subject\ to\ Sv = 0} \\ &\mathbf{and\ lb_i < v_i < ub_i} \end{aligned} \qquad \text{Eq 1.1}$$

Soon after Edwards' *E. coli* Model, models involving yeast and other microbes were developed [27]. Furthermore, the development of the OptKnock technique allowed for easier analysis of gene deletions, leading to the analysis of gene essentiality and the spinoff of many other specialized *E. coli* GEMs [28, 29]. New formulations of FBA were also developed, including dynamic FBA (dFBA) which allowed for an unsteady state consumption of nutrients from the bacteria's microenvironment, parsimonious FBA (pFBA) which yielded a single solution with minimized fluxes, and Flux Variability Analysis (FVA) which allowed for exploration of the boundaries of the multidimensional flux space [30, 31].

Developments in these GEMs and recombinant DNA technology eventually allowed these bacteria to be synthetically modified to produce industrially useful chemicals, and even cannabinoids [32]. Currently, reconstructions are created by surveying databases for gene-annotated information, converting data into a mathematical model, and iteratively updating these models with phenotypic and experimental data [33]. A recent tool for assessing the quality of GEMs, MEMOTE, was developed to help further improve the qualities of these network reconstructions [34]. Furthermore, these bacterial GEMs influenced some groups to apply the same concept to humans, resulting in human reconstructions.

1.3 Human Reconstructions

Whereas bacterial GEMs were used primarily for industrial purposes, human GEMs are more useful in identifying drug targets for treating various diseases [35]. The journey to creating a human genome reconstruction began with Romero's work in developing a pathway-genome database known as HumanCyc [36]. This was not a network reconstruction, but created an important database for future models. Drawing information from various databases including Kyoto Encyclopedia of Genes and Genomes (KEGG) and National Center for Biotechnology Information's EntrezGene, the first human reconstruction was developed by Duarte in 2007 known as Recon 1 [37]. This reconstruction had many gaps, yet it was able to provide initial information about altered metabolic states that can lead to diseases, elucidating drug targets for treatment. With the development of standardized genome reconstruction techniques and the COnstraint-Based Reconstruction and Analysis (COBRA) toolbox, more quantitative predictions of cellular metabolism became available, further improving the analysis of network reconstructions [38, 39].

Soon after Recon 1, another human reconstruction known as the Edinburgh Human Metabolic Network (EHMN) surfaced after drawing data from KEGG and HumanCyc [40]. Here, Ma and colleagues tried to consolidate some inconsistencies that existed with Enzyme Commission numbers and identified the presence of essential metabolites that have no synthesis pathways in the human body, an important finding for nutritional studies. The genes identified in these models would then serve to be important predictors for disease models, as over 95.72% of the genes in EHMN were predictors of various diseases [40].

Nearly half a decade later, the differences between Recon1 and EHMN were reconciled in Recon2, along with information from other databases including HepatoNet1, AcFaO-module, and small intestine enterocyte reconstructions [41]. With a similar goal of identifying disease treatments, Recon2 predicted for the biomarkers (metabolites) associated with inborn errors of metabolism (IEM). Furthermore, Recon2 dramatically expanded the size of the network reconstruction to include 7440 reactions.

After recognizing the importance of consolidating the omics studies and providing consistency, the Human Metabolic Reconstruction was created with the first searchable database and accompanying website [42]. Recon 2 would be later updated to Recon 2.2 to assist in ATP calculations, and there was increasing interest on the effect of the microbiota on human metabolism via the development of AGORA (Assembly of Gut Organisms through Reconstruction and Analysis) [43-45].

In 2018, human reconstruction models received yet another update in the form of Recon3D, with its accompanying website (https://www.vmh.life/), the Virtual Metabolic Human (VMH) [46]. Here, microbiota information was further developed and incorporated with nutritional data, allowing for the analysis of various diets on human metabolism [47]. Most recently, a consolidation of the HMR and Recon lineages of human reconstruction was published under the name Human1 with its accompanying website (https://www.metabolicatlas.org/) [48]. Human1 achieved the impressive feat of 100% stoichiometric consistency with its reactions, and 99.4% and 98.2% consistency for mass and charge balance, respectively. Furthermore, Human1 allows for comparisons between healthy and tumor tissue, further improving the drug targeting of chemotherapeutics. Lastly, the Harvey-Harvetta model developed by Thiele serves to integrate the physiology of organs with previously developed GEMs [49]. These physiological models further compartmentalize reactions to specific organs and allow for the constraint of inter-organ transport equations, allowing for integration with traditional PBPK models to make the reactions even more realistic.

The development of various human reconstructions can be tracked in *Table 1.1*. Overall, the presence of human reconstructions serves an important function in the development of precision medicine, in which a person's metabotype is useful to interpret the overall health status, expanding upon the limited number of metabolites that are currently clinically tested [50]. Through these reconstructions, IEMs can be predicted for newborns based on blood sampling, drug effects (and side-effects) can be predicted, and interactions between individuals and their microbiota can be elucidated [50].

Table 1.1 History of Human Reconstruction Development

Model	Metabolites	Reactions	Genes/Enzymes
HumanCyc (2004) [36]	?	896	2709
Recon 1 (2007) [37]	2712	3311	2004
EHMN (2007) [40]	2671	2823	2322
Recon 2 (2013) [41]	2626	7440	1789
Recon 2.2 (2016) [43]	5324	7785	1675
Recon 3D (2018) [46]	4140	13543	12890
VMH (2018) [46]	5180	17730	3695
Human1 (2020) [48]	10138	13417	3625
Harvey-Harvetta (2020) [49]	56452	81094	2071

1.4 Multiscale Modelling and Integration

With PBPK models predicting the ADME of drugs through the body, and GEMs predicting the metabolism of various compounds in the body, it makes sense to integrate GEM information into the PBPK models to better predict drug clearance rates in situations where human kinetic data is not readily available. In his thesis, Toroghi began the work on model integration by including fluxes from HepatoNet1 in the liver for various reactions in the PBPK model [51]. Specifically, the models are integrated with dFBA such that the concentration of a metabolite is used to predict the maximum reaction rate per Michaelis-Menten kinetics for constraining the fluxes in HepatoNet1 (See *Figure 1.1*, Eq. 1.2) [30][31]. In this work, since the maximum rates assigned to enzymes responsible for metabolism are used as constraints in the Harvey model, and the fluxes solved with Harvey are then used to update the concentration values in various tissues (Eq. 1.3). This approach is used in this thesis to predict for the metabolism of various metabolites.

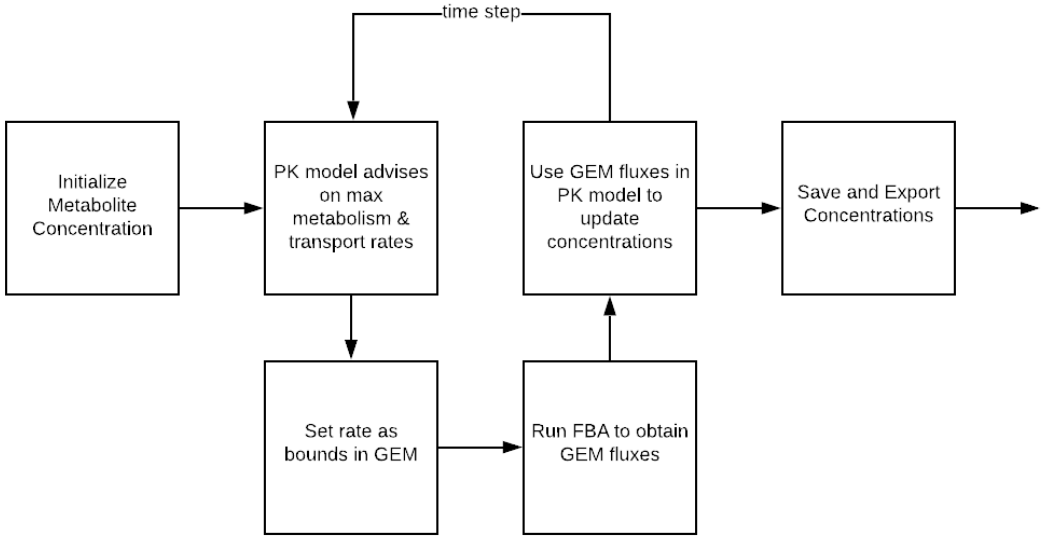

Fig. 1.1 Schematic for dynamic Flux Balance Analysis

$$\begin{aligned} &\mathbf{max} \quad \mathbf{f^T v} \\ &\mathbf{subject\ to\ Sv = 0} \\ &\mathbf{and\ lb_i < v_i < ub_i} \end{aligned} \qquad \text{Eq 1.2}$$

$$\mathbf{ub_i} = \frac{\mathbf{V_{max} C_i}}{\mathbf{K_m + C_i}} \qquad \text{Eq.1.3}$$

1.5 Metabolism of Tetrahydrocannabinol

Tetrahydrocannabinol (THC) and cannabidiol (CBD) are two of the major phytocannabinoids found in the plant *Cannabis sativa*. These molecules interact with the cannabinoid class of G-protein coupled receptors (CB1, CB2) in the body through the recently discovered endocannabinoid system [52]. CB1 is primarily found in the central nervous system, whereas CB2 is found along immune cells. The work presented in this thesis will focus on THC, as it is the psychoactive cannabinoid whereas CBD is responsible for more immunomodulatory effects [52].

THC is a highly lipophilic substance (logP =5.648) which is readily taken up by highly perfused tissue such as the heart, lungs, liver, and brain [53]. It has poor plasma solubility and 95-99% of plasma THC is bound to lipoproteins. THC is a psychoactive compound that affects working memory and can lead to conceptual disorganization, hallucinations, blunted affect, somatic concern, motor retardation and poor attention [52, 54-56]. It has also been implicated in differential DNA methylation patterns, leading to epigenetic effects [57].

THC is metabolized by many different CYP-450 enzymes, many of which concentrated at the liver [58]. It its phase I metabolism, THC is primarily metabolized by P450 enzyme CYP2C9 into 11-hydroxy tetrahydrocannabinol (11-OH-THC) and further metabolized by CYP2C9 into 11-nor-9-carboxy tetrahydrocannabinol (THC-COOH). Afterwards, in phase II metabolism THC-COOH is glucuronidated by UDP glucuronosyltransferases into THC-COOH-Glucuronide to increase its solubility in urine, allowing for excretion via the kidneys [59, 60]. 11-OH-THC is also excreted in the feces [52].

Depending on an individual's CYP2C9 genotype, variations in this metabolism could also occur. Specifically, the CYP2C9 Enzyme has 3 isoforms: CYP2C9.1 (Arg144), CYP2C9.2 (Cys144) and CYP2C9.3 (Leu359) [61]. These polymorphisms have been implicated in differences in the maximum blood concentration (Cmax), the time that Cmax is reached (Tmax), and the overall drug exposure from the area under the curve (AUC) [62].

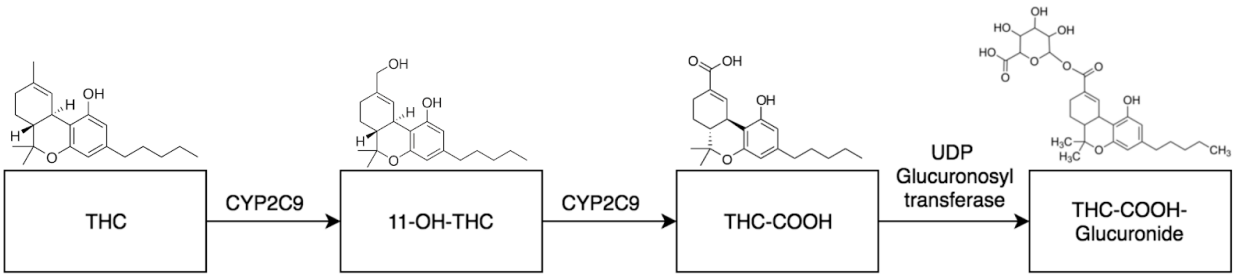

Fig. 1.2 Primary metabolic pathway for tetrahydrocannabinol

The introduction of cannabis as a legalized recreational drug in Canada has led to significant changes in public health policy. With ethanol, there are many models that predict the absorption, distribution, metabolism, and elimination (ADME) of the drug, and there are guidelines advising on the "rule of thumb" of metabolising approximately 1 standard 14g drink per hour. However, the ADME of the primary psychoactive compound in cannabis, tetrahydrocannabinol (THC), is poorly understood. It should be noted that 11-hydroxy-tetrahydrocannabinol is also psychoactive. There have been recent attempts to develop a standardized THC unit to better regulate the industry and much work on the newly discovered endocannabinoid system to understand the pharmacokinetics of various cannabinoids [59].

Current work on understanding THC metabolism involved clinical trials to elucidate pharmacokinetic parameters, as well as driving studies to gauge the psychomotor effects. Given its multiple forms of intake including inhalation, oral, sublingual, rectal, transcutaneous, and intravenous all having different pharmacokinetic properties, it is especially difficult to well characterize its metabolism [53]. Pharmacokinetic models for THC metabolism have been made, but they suffer from not characterizing the whole body, lack of absorption kinetics, or are animal models [63-67]. Thus, this thesis seeks to make a whole-body PBPK model for THC metabolism that can include the impact of diseased states to better extend its practical use in medicine [68,69].

1.6 Metabolism of Ethanol

Ethanol is a drug that has been extensively studied and is one of the most widely-used drugs in the world today [70]. Ethanol abuse can lead to dependence, liver cirrhosis, social withdrawal, and serious implications when driving under the influence [70].

It is understood that ethanol is primarily eliminated by liver alcohol dehydrogenase (ADH) along with other enzymes into the compound acetaldehyde, which is in turn primarily eliminated by mitochondrial aldehyde dehydrogenase (ALDH2) into acetate [71-74]. Other processes involved in alcohol metabolism include Microsomal Ethanol Oxidizing Systems (namely cytochrome P450 enzyme 2E1), catalase, peroxisomes, and non-oxidative methods such as Fatty Acid Ethyl Esters [73-76] Acetaldehyde is a toxic metabolite whose buildup can cause symptoms of facial flushing, headaches, nausea, dizziness, and tachycardia and its elimination by ALDH2 is heavily influenced by genetic polymorphisms [74].

The pharmacokinetics of ethanol have been well characterized in literature since Widmark's research in 1933 assuming 0th order elimination [77,78]. This work was expanded upon by Lundquist and Wolthers, who incorporated Michaelis-Menten Kinetics to describe the non-linearity of elimination curves below 0.2mg/mL. In the late 1900s, further research on ethanol metabolism has indicated that the concentration of ethanol in the blood after ingestion is proportional to the total amount of body water, and that first-pass metabolism by the stomach does not make a significant contribution to ethanol metabolism in fasted patients [78-82]. In fed patients, the back-up of the gastric valves retains more ethanol in the stomach, leading to more first-pass metabolism. Aside from metabolism, ethanol is also exchanged through the breath, sweat, and urine in lower amounts [83].

Given that the enzymes for metabolizing ethanol are well characterized in the Harvey Model, ethanol and acetaldehyde were chosen as the metabolites of choice for integrating PBPK and GEM models.

1.7 References

[1]T. Teorell, 'Kinetics of distribution of substances administered to the body, I : The extravascular modes of administration', Archives internationales de pharmacodynamie et de therapie, vol. 57, pp. 205–225, 1937.

[2] P. Zhao *et al.*, "Applications of physiologically based pharmacokinetic (PBPK) modeling and simulation during regulatory review," *Clin. Pharmacol. Ther.*, vol. 89, no. 2, pp. 259–267, 2011, doi: 10.1038/clpt.2010.298.

[3] K. B. Bischoff, R. L. Dedrick, D. S. Zaharko, and J. A. Longstreth, "Methotrexate pharmacokinetics," *J. Pharm. Sci.*, vol. 60, no. 8, pp. 1128–1133, 1971, doi: 10.1002/jps.2600600803.

[4] R. P. Brown, M. D. Delp, S. L. Lindstedt, L. R. Rhomberg, and R. P. Beliles, "Physiological parameter values for physiologically based pharmacokinetic models," *Toxicol. Ind. Health*, 1997, doi: 10.1177/074823379701300401.

[5] [1] J. E. Sager, J. Yu, I. Ragueneau-Majlessi, and N. Isoherranen, "Physiologically based pharmacokinetic (PBPK) modeling and simulation approaches: A systematic review of published models, applications, and model verification," *Drug Metab. Dispos.*, vol. 43, no. 11, pp. 1823–1837, 2015, doi: 10.1124/dmd.115.065920.

[6] P. Poulin and F. P. Theil, "A priori prediction of tissue: Plasma partition coefficients of drugs to facilitate the use of physiologically-based pharmacokinetic models in drug discovery," *J. Pharm. Sci.*, vol. 89, no. 1, pp. 16–35, 2000, doi: 10.1002/(SICI)1520-6017(200001)89:1<16::AID-JPS3>3.0.CO;2-E.

[7] T. Rodgers and M. Rowland, "Physiologically based pharmacokinetic modeling 2: Predicting the Tissue Distribution of Acids, Very Weak Bases, N. and Z. Molecular Nanomedicine Towards Cancer," *J. Pharm. Sci.*, vol. 95, no. 6, pp. 1238–1257, 2006, doi: 10.1002/jps.20502

[8] T. Rodgers, D. Leahy, and M. Rowland, "Physiologically based pharmacokinetic modeling 1: Predicting the tissue distribution of moderate-to-strong bases," *J. Pharm. Sci.*, vol. 94, no. 6, pp. 1259–1276, 2005, doi: 10.1002/jps.20322.

[9] A. M. Ahmad, "Potential pharmacokinetic interactions between antiretrovirals and medicinal plants used as complementary and African traditional medicines," *Biopharm. Drug Dispos.*, vol. 28, no. 3, pp. 135–143, 2007, doi: 10.1002/bdd.

[10] H. M. Jones, I. B. Gardner, and K. J. Watson, "Modelling and PBPK simulation in drug discovery," *AAPS J.*, vol. 11, no. 1, pp. 155–166, 2009, doi: 10.1208/s12248-009-9088-1.

[11] C. Wagner *et al.*, "Application of physiologically based pharmacokinetic (PBPK) modeling to support dose selection: Report of an FDA public workshop on PBPK," *CPT Pharmacometrics Syst. Pharmacol.*, vol. 4, no. 4, pp. 226–230, 2015, doi: 10.1002/psp4.33.

[12] M. Jamei, "Recent Advances in Development and Application of Physiologically-Based Pharmacokinetic (PBPK) Models: a Transition from Academic Curiosity to Regulatory Acceptance," *Curr. Pharmacol. Reports*, vol. 2, no. 3, pp. 161–169, 2016, doi: 10.1007/s40495-016-0059-9.

[13] M. Rowland, C. Peck, and G. Tucker, "Physiologically-Based Pharmacokinetics in Drug Development and Regulatory Science," *Annu. Rev. Pharmacol. Toxicol.*, vol. 51, no. 1, pp. 45–73, 2011, doi: 10.1146/annurev-pharmtox-010510-100540.

[14] H. M. Jones *et al.*, "Application of PBPK modelling in drug discovery and development at Pfizer," *Xenobiotica*, vol. 42, no. 1, pp. 94–106, 2012, doi: 10.3109/00498254.2011.627477.

[15] T. Saeheng, K. Na-Bangchang, and J. Karbwang, “Utility of physiologically based pharmacokinetic (PBPK) modeling in oncology drug development and its accuracy: a systematic review,” *Eur. J. Clin. Pharmacol.*, vol. 74, no. 11, pp. 1365–1376, 2018, doi: 10.1007/s00228-018-2513-6.
[16] M. Siccardi, S. Rannard, and A. Owen, “The emerging role of physiologically based pharmacokinetic modelling in solid drug nanoparticle translation,” *Adv. Drug Deliv. Rev.*, vol. 131, pp. 116–121, 2018, doi: 10.1016/j.addr.2018.06.016.
[17] E. D. G. Garessus, H. Mielke, and U. Gundert-Remy, “Exposure of Infants to Isoniazid via Breast Milk after Maternal Drug Intake of Recommended Doses Is Clinically Insignificant Irrespective of Metaboliser Status. A Physiologically-Based Pharmacokinetic (PBPK) Modelling Approach to Estimate Drug Exposure of,” *Front. Pharmacol.*, vol. 9, no. JAN, pp. 1–13, 2019, doi: 10.3389/fphar.2019.00005.
[18] C. Hartmanshenn, M. Scherholz, and I. P. Androulakis, “Physiologically-based pharmacokinetic models: approaches for enabling personalized medicine,” *J. Pharmacokinet. Pharmacodyn.*, vol. 43, no. 5, pp. 481–504, 2016, doi: 10.1007/s10928-016-9492-y.
[19] N. Marsousi, J. A. Desmeules, S. Rudaz, and Y. Daali, “Usefulness of PBPK Modeling in Incorporation of Clinical Conditions in Personalized Medicine,” *J. Pharm. Sci.*, vol. 106, no. 9, pp. 2380–2391, 2017, doi: 10.1016/j.xphs.2017.04.035.
[20] M. Chetty, T. N. Johnson, S. Polak, F. Salem, K. Doki, and A. Rostami-Hodjegan, “Physiologically based pharmacokinetic modelling to guide drug delivery in older people,” *Adv. Drug Deliv. Rev.*, vol. 135, pp. 85–96, 2018, doi: 10.1016/j.addr.2018.08.013.
[21] A. Rostami-Hodjegan, “Reverse Translation in PBPK and QSP: Going Backwards in Order to Go Forward With Confidence,” *Clin. Pharmacol. Ther.*, vol. 103, no. 2, pp. 224–232, 2018, doi: 10.1002/cpt.904.
[22] C. Perry, G. Davis, T. M. Conner, and T. Zhang, “Utilization of Physiologically Based Pharmacokinetic Modeling in Clinical Pharmacology and Therapeutics: an Overview,” *Curr. Pharmacol. Reports*, 2020, doi: 10.1007/s40495-020-00212-x.
[23] J. S. Edwards and B. O. Palsson, “Systems properties of the Haemophilus influenzae Rd metabolic genotype,” *J. Biol. Chem.*, vol. 274, no. 25, pp. 17410–17416, 1999, doi: 10.1074/jbc.274.25.17410.
[24] J. S. Edwards and B. O. Palsson, “The Escherichia coli MG1655 in silico metabolic genotype: Its definition, characteristics, and capabilities,” *Proc. Natl. Acad. Sci. U. S. A.*, vol. 97, no. 10, pp. 5528–5533, 2000, doi: 10.1073/pnas.97.10.5528.
[25] J. D. Orth, I. Thiele, and B. O. Palsson, “What is flux balance analysis?,” *Nat. Biotechnol.*, vol. 28, no. 3, pp. 245–248, 2010, doi: 10.1038/nbt.1614.
[26] J. M. Walker, T. Douglas, and I. Carrell and Kenneth, *Neisseria Meningitidis: Advanced Methods and Protocols*, vol. 531, no. 1. 2009.
[27] T. Doerks, R. R. Copley, J. Schultz, C. P. Ponting, and P. Bork, “Systematic identification of novel protein domain families associated with nuclear functions,” *Genome Res.*, vol. 12, no. 1, pp. 47–56, 2002, doi: 10.1101/gr.203201.
[28] A. P. Burgard, P. Pharkya, and C. D. Maranas, “OptKnock: A Bilevel Programming Framework for Identifying Gene Knockout Strategies for Microbial Strain Optimization,” *Biotechnol. Bioeng.*, vol. 84, no. 6, pp. 647–657, 2003, doi: 10.1002/bit.10803.
[29] A. L. Osterman and S. Y. Gerdes, *Microbial Gene Essentiality - Protocols and Bioinformatics: Preface*, vol. 416. 2007.

[30] R. Mahadevan, J. S. Edwards, and F. J. Doyle, “Dynamic flux balance analysis of diauxic growth,” *Biophys. J.*, vol. 83, no. 3, pp. 1331–1340, 2002, [Online]. Available: https://pdfs.semanticscholar.org/8d56/a26c56704266b5d7c426ecdfc286962f9112.pdf.
[31] J. A. Gomez, K. Höffner, and P. I. Barton, “DFBAlab: A fast and reliable MATLAB code for dynamic flux balance analysis,” *BMC Bioinformatics*, vol. 15, no. 1, pp. 1–10, 2014, doi: 10.1186/s12859-014-0409-8.
[32] X. Luo et al., "Author Correction: Complete biosynthesis of cannabinoids and their unnatural analogues in yeast", *Nature*, vol. 580, no. 7802, pp. E2-E2, 2020. Available: 10.1038/s41586-020-2109-z.
[33] M. A. Oberhardt, B. Palsson, and J. A. Papin, “Applications of genome-scale metabolic reconstructions,” *Mol. Syst. Biol.*, vol. 5, no. 320, pp. 1–15, 2009, doi: 10.1038/msb.2009.77.
[34] C. Lieven *et al.*, “MEMOTE for standardized genome-scale metabolic model testing,” *Nat. Biotechnol.*, vol. 38, no. 3, pp. 272–276, 2020, doi: 10.1038/s41587-020-0446-y.
[35] A. Mardinoglu, R. Agren, C. Kampf, A. Asplund, M. Uhlen, and J. Nielsen, “Genome-scale metabolic modelling of hepatocytes reveals serine deficiency in patients with non-alcoholic fatty liver disease,” *Nat. Commun.*, vol. 5, no. May 2013, pp. 1–11, 2014, doi: 10.1038/ncomms4083.
[36] P. Romero, J. Wagg, M. L. Green, D. Kaiser, M. Krummenacker, and P. D. Karp, “Computational prediction of human metabolic pathways from the complete human genome.,” *Genome Biol.*, vol. 6, no. 1, pp. 1–17, 2005, doi: 10.1186/gb-2004-6-1-r2.
[37] N. C. Duarte *et al.*, “Global reconstruction of the human metabolic network based on genomic and bibliomic data,” *Proc. Natl. Acad. Sci. U. S. A.*, vol. 104, no. 6, pp. 1777–1782, 2007, doi: 10.1073/pnas.0610772104.
[38] I. Thiele and B. Palsson, “A protocol for generating a high-quality genome-scale metabolic reconstruction,” *Nat. Protoc.*, vol. 5, no. 1, pp. 93–121, 2010, doi: 10.1038/nprot.2009.203.
[39] J. Schellenberger et al., "Quantitative prediction of cellular metabolism with constraint-based models: the COBRA Toolbox v2.0", *Nature Protocols*, vol. 6, no. 9, pp. 1290-1307, 2011. Available: 10.1038/nprot.2011.308.
[40] H. Ma *et al.*, “The Edinburgh human metabolic network reconstruction and its functional analysis,” *Mol. Syst. Biol.*, vol. 3, no. 135, pp. 1–8, 2007, doi: 10.1038/msb4100177.
[41] I. Thiele *et al.*, “A community-driven global reconstruction of human metabolism,” *Nikolaus Sonnenschein*, vol. 17, no. 5, p. 34, 2013, doi: 10.1038/nbt.2488.
[42] N. Pornputtapong, I. Nookaew, and J. Nielsen, “Human metabolic atlas: An online resource for human metabolism,” *Database*, vol. 2015, pp. 1–9, 2015, doi: 10.1093/database/bav068.
[43] N. Swainston *et al.*, “Recon 2.2: from reconstruction to model of human metabolism,” *Metabolomics*, vol. 12, no. 7, 2016, doi: 10.1007/s11306-016-1051-4.
[44] C. Zhang and Q. Hua, “Applications of genome-scale metabolic models in biotechnology and systems medicine,” *Front. Physiol.*, vol. 6, no. JAN, pp. 1–8, 2016, doi: 10.3389/fphys.2015.00413.
[45] S. Magnúsdóttir *et al.*, “Generation of genome-scale metabolic reconstructions for 773 members of the human gut microbiota,” *Nat. Biotechnol.*, vol. 35, no. 1, pp. 81–89, 2017, doi: 10.1038/nbt.3703.
[46] E. Brunk *et al.*, “Recon3D enables a three-dimensional view of gene variation in human metabolism,” *Nat. Biotechnol.*, vol. 36, no. 3, pp. 272–281, 2018, doi: 10.1038/nbt.4072.

[47] A. Noronha *et al.*, “The Virtual Metabolic Human database: Integrating human and gut microbiome metabolism with nutrition and disease,” *Nucleic Acids Res.*, vol. 47, no. D1, pp. D614–D624, 2019, doi: 10.1093/nar/gky992.
[48] J. L. Robinson *et al.*, “An atlas of human metabolism,” *Sci. Signal.*, vol. 13, no. 624, pp. 1–12, 2020, doi: 10.1126/scisignal.aaz1482.
[49] I. Thiele et al., "Personalized whole-body models integrate metabolism, physiology, and the gut microbiome", *Molecular Systems Biology*, vol. 16, no. 5, 2020. Available: 10.15252/msb.20198982.
[50] R. D. Beger *et al.*, “Metabolomics enables precision medicine: ‘A White Paper, Community Perspective,’” *Metabolomics*, vol. 12, no. 10, 2016, doi: 10.1007/s11306-016-1094-6.
[51] M. Toroghi, W. Cluett and R. Mahadevan, "A Multi-Scale Model of the Whole Human Body based on Dynamic Parsimonious Flux Balance Analysis", *IFAC-PapersOnLine*, vol. 49, no. 7, pp. 937-942, 2016. Available: 10.1016/j.ifacol.2016.07.319.
[52] P. Sharma, P. Murthy, and M. M. S. Bharath, “Chemistry, metabolism, and toxicology of cannabis: Clinical implications,” *Iran. J. Psychiatry*, vol. 7, no. 4, pp. 149–156, 2012.
[53] M. A. Huestis, “Human cannabinoid pharmacokinetics,” *Chem. Biodivers.*, vol. 4, no. 8, pp. 1770–1804, 2007, doi: 10.1002/cbdv.200790152.
[54] S. Ganesh, J. Cortes-Briones, M. Ranganathan, R. Radhakrishnan, P. D. Skosnik, and D. C. D’Souza, “Psychosis-relevant effects of intravenous delta-9-tetrahydrocannabinol - A mega analysis of individual participant-data from human laboratory studies,” *Int. J. Neuropsychopharmacol.*, vol. 0, pp. 1–33, 2020, doi: 10.1093/ijnp/pyaa031.
[55] Association, P. S. H. & S. Cannabis in the Workplace. Public Serv. Heal. Saf. Assoc. 2020, 66, 317–318.
[56] K. C. S. Adam, M. K. Doss, E. Pabon, E. K. Vogel, and H. de Wit, “Δ9-Tetrahydrocannabinol (THC) impairs visual working memory performance: a randomized crossover trial,” *Neuropsychopharmacology*, pp. 0–1, 2020, doi: 10.1038/s41386-020-0690-3.
[57] A. J. Osborne *et al.*, “Genome-wide DNA methylation analysis of heavy cannabis use in a New Zealand longitudinal cohort,” *bioRxiv*, p. 829598, 2019, doi: 10.1101/829598.
[58] K. Watanabe, S. Yamaori, T. Funahashi, T. Kimura, and I. Yamamoto, “Cytochrome P450 enzymes involved in the metabolism of tetrahydrocannabinols and cannabinol by human hepatic microsomes,” *Life Sci.*, vol. 80, no. 15, pp. 1415–1419, 2007, doi: 10.1016/j.lfs.2006.12.032.
[59] S. M. Stout and N. M. Cimino, “Exogenous cannabinoids as substrates, inhibitors, and inducers of human drug metabolizing enzymes: A systematic review,” *Drug Metab. Rev.*, vol. 46, no. 1, pp. 86–95, 2014, doi: 10.3109/03602532.2013.849268.
[60] T. R. Spindle *et al.*, “Urinary Excretion Profile of 11-Nor-9-Carboxy-Δ9-Tetrahydrocannabinol (THCCOOH) Following Smoked and Vaporized Cannabis Administration in Infrequent Cannabis Users,” *J. Anal. Toxicol.*, vol. 44, no. 1, pp. 1–14, 2020, doi: 10.1093/jat/bkz038.
[61] T. M. Bland, R. L. Haining, T. S. Tracy, and P. S. Callery, “CYP2C-catalyzed delta(9)-tetrahydrocannabinol metabolism: Kinetics, pharmacogenetics and interaction with phenytoin,” *Biochem. Pharmacol.*, vol. 70, no. 7, pp. 1096–1103, 2005, doi: 10.1016/j.bcp.2005.07.007.
[62] C. Sachse-Seeboth *et al.*, “Interindividual variation in the pharmacokinetics of Δ9-tetrahydrocannabinol as related to genetic polymorphisms in CYP2C9,” *Clin. Pharmacol. Ther.*, vol. 85, no. 3, pp. 273–276, 2009, doi: 10.1038/clpt.2008.213.

[63] A. Marsot, C. Audebert, L. Attolini, B. Lacarelle, J. Micallef, and O. Blin, “Population pharmacokinetics model of THC used by pulmonary route in occasional cannabis smokers,” *J. Pharmacol. Toxicol. Methods*, vol. 85, pp. 49–54, 2017, doi: 10.1016/j.vascn.2017.02.003.
[64] J. A. A. C. Heuberger *et al.*, “Population Pharmacokinetic Model of THC Integrates Oral, Intravenous, and Pulmonary Dosing and Characterizes Short- and Long-term Pharmacokinetics,” *Clin. Pharmacokinet.*, vol. 54, no. 2, pp. 209–219, 2015, doi: 10.1007/s40262-014-0195-5.
[65] W. R. Wolowich, R. Greif, M. Kleine-Brueggeney, W. Bernhard, and L. Theiler, “Minimal Physiologically Based Pharmacokinetic Model of Intravenously and Orally Administered Delta-9-Tetrahydrocannabinol in Healthy Volunteers,” *Eur. J. Drug Metab. Pharmacokinet.*, vol. 44, no. 5, pp. 691–711, 2019, doi: 10.1007/s13318-019-00559-7.
[66] J. Methaneethorn, K. Naosang, P. Kaewworasut, C. Poomsaidorn, and M. Lohitnavy, “Development of a Physiologically-Based Pharmacokinetic Model of Δ9-Tetrahydrocannabinol in Mice, Rats, and Pigs,” *Eur. J. Drug Metab. Pharmacokinet.*, no. 0123456789, 2020, doi: 10.1007/s13318-020-00616-6.
[67] R. Awasthi, G. An, M. D. Donovan, and L. L. Boles Ponto, “Relating Observed Psychoactive Effects to the Plasma Concentrations of Delta-9-Tetrahydrocannabinol and Its Active Metabolite: An Effect-Compartment Modeling Approach,” *J. Pharm. Sci.*, vol. 107, no. 2, pp. 745–755, 2018, doi: 10.1016/j.xphs.2017.09.009.
[68] B. C. Ginsburg, “Toward a Comprehensive Model of Δ9-Tetrahydrocannabinol Pharmacokinetics Using a Population Pharmacokinetics Approach,” *Clin. Pharmacokinet.*, vol. 54, no. 2, pp. 129–131, 2015, doi: 10.1007/s40262-014-0210-x.
[69] C. A. MacCallum and E. B. Russo, “Practical considerations in medical cannabis administration and dosing,” *Eur. J. Intern. Med.*, vol. 49, no. October 2017, pp. 12–19, 2018, doi: 10.1016/j.ejim.2018.01.004.
[70] World Health Organization, ‘‘Global status report on alcohol and health,’’ WHO Library Cataloguing, vol. 978, pp. 1–61, Apr. 2014.
[71] R. Rajendram, R. Rajendram, and V. R. Preedy, *Ethanol Metabolism and Implications for Disease*, vol. 1. Elsevier Inc., 2016.
[72] J. A. Hernández, R. C. López-Sánchez, and A. Rendón-Ramírez, “Lipids and Oxidative Stress Associated with Ethanol-Induced Neurological Damage,” *Oxid. Med. Cell. Longev.*, vol. 2016, no. Table 1, 2016, doi: 10.1155/2016/1543809.
[73] C. Heier, H. Xie, and R. Zimmermann, “Nonoxidative ethanol metabolism in humans—from biomarkers to bioactive lipids,” *IUBMB Life*, vol. 68, no. 12, pp. 916–923, 2016, doi: 10.1002/iub.1569.
[74] A. Cederbaum, “Alcohol Metabolism,” *Clin Liver Dis*, vol. 16, no. 4, pp. 1–11, 2012, doi: 10.1016/j.cld.2012.08.002.ALCOHOL.
[75] C. Wright and R. Moore, "Disulfiram treatment of alcoholism", *The American Journal of Medicine*, vol. 88, no. 6, pp. 647-655, 1990. Available: 10.1016/0002-9343(90)90534-k.
[76] C. S. Lieber, “The discovery of the microsomal ethanol oxidizing system and its physiologic and pathologic role,” *Drug Metab. Rev.*, vol. 36, no. 3–4, pp. 511–529, 2004, doi: 10.1081/DMR-200033441.
[77] P. K. Wilkinson, “Pharmacokinetics of Ethanol: A Review,” *Alcohol. Clin. Exp. Res.*, vol. 4, no. 1, pp. 6–21, 1980, doi: 10.1111/j.1530-0277.1980.tb04785.x.

[78] P. E. Watson, I. D. Watson, and R. D. Batt, “Prediction of blood alcohol concentrations in human subjects. Updating the Widmark equation,” *J. Stud. Alcohol*, vol. 42, no. 7, pp. 547–556, 1981, doi: 10.15288/jsa.1981.42.547.
[79] D. W. Crabb, W. F. Bosron, and T. K. Li, “Ethanol metabolism,” *Pharmacol. Ther.*, vol. 34, no. 1, pp. 59–73, 1987, doi: 10.1016/0163-7258(87)90092-1.
[80] R. P. Roine, R. T. Gentry, R. T. Lim, E. Baraona, and C. S. Lieber, “Effect of Concentration of Ingested Ethanol on Blood Alcohol Levels,” *Alcohol. Clin. Exp. Res.*, vol. 15, no. 4, pp. 734–738, 1991, doi: 10.1111/j.1530-0277.1991.tb00589.x.
[81] A. S. ,. J. M. Brown *et al.*, “The effect of gastritis on human gastric alcohol dehydrogenase activity and ethanol metabolism,” *Aliment. Pharmacol. Ther.*, vol. 9, no. 1, pp. 57–61, 1995, doi: 10.1111/j.1365-2036.1995.tb00352.x.
[82] M. D. Levitt, R. Li, E. G. Demaster, M. Elson, J. Furne, and D. G. Levitt, “Use of measurements of ethanol absorption from stomach and intestine to assess human ethanol metabolism,” *Am. J. Physiol. - Gastrointest. Liver Physiol.*, vol. 273, no. 4 36-4, 1997, doi: 10.1152/ajpgi.1997.273.4.g951.
[83] V. A. Ramchandani, W. F. Bosron, and T. K. Li, “Research advances in ethanol metabolism,” *Pathol. Biol.*, vol. 49, no. 9, pp. 676–682, 2001, doi: 10.1016/S0369-8114(01)00232-2.

2 Hypothesis and Objectives

2.1 Motivation

Ethanol and cannabis use is widespread and understanding how these drugs affect the body to provide safe guidelines for their usage is imperative. To better advise on these guidelines, lessons can be drawn from both the pharmaceutical and bioengineering industries to develop a model that incorporates both pharmacokinetic and genomic modelling, culminating in personalizable models of drug metabolism. By predicting the concentration of ethanol and tetrahydrocannabinol (THC) in the body, guidelines involving their safe consumption can be updated and individuals can be more informed about their usage.

2.2 Hypothesis

By gap-filling enzyme-specific Physiologically-Based Pharmacokinetic (PBPK) models with general metabolic fluxes from Genome-scale Models (GEM), we can predict the impact of inter-individual variations on the clinical pharmacokinetics of tetrahydrocannabinol (THC) and ethanol metabolism.

2.3 Objectives

1. Develop a PBPK model for THC with population-based polymorphic CYP2C9 enzyme kinetics to advise on classes of individuals with varying susceptibility to cannabis.
2. Integrate a previously developed Ethanol model with a genome-scale human metabolism model to better inform on the effect of interindividual variations in exposure to ethanol and its metabolites.

3 Physiologically-Based Pharmacokinetic Model for Predicting Blood and Tissue Tetrahydrocannabinol Concentrations

3.1 Abstract

The introduction of cannabis as a legalized recreational drug in Canada has led to significant changes in public health policy. Tetrahydrocannabinol (THC) is the primary psychoactive compound in cannabis and its absorption, distribution, metabolism, and elimination are poorly understood. The use of THC can impair an individual's ability to operate a motor vehicle, leading to an increased risk of accidents. Thus, additional research must be conducted to gauge the inter-individual differences in effect and duration of THC's effect. In this study, a comprehensive whole-body physiologically-based pharmacokinetic (PBPK) model for THC metabolism was developed to track blood THC concentrations accounting for interindividual variations such as age, sex, body composition, bioavailability and drug metabolizing enzyme (DME) polymorphisms after various dosages. This model was fitted and validated with clinical human cannabis smoking data. Using this model, we found effects of various factors on THC concentrations in different tissue compartments, and that the wild-type form of Cytochrome P450 2C9 (CYP2C9) DME showed faster metabolism of THC than other isoforms. The nature of the our PBPK model allowed for the investigation of non-blood compartments as well. To gauge the effects on driving, we compared the Standard Deviation of Lateral Position under the effects of THC and ethanol, and found that ethanol has a stronger but shorter-lasting effect. We anticipate that this model can be used to better predict the effects of a "standard THC unit" and help advise public health policies for safe cannabis usage.

3.2 Introduction

The introduction of cannabis as a legalized recreational drug in Canada has led to significant changes in public health policy. With other recreational drugs such as ethanol, there are many models that predict the absorption, distribution, metabolism, and elimination (ADME) of the drug [1–5], and there are guidelines advising on general rule of metabolizing one to two standard drinks per hour [6–8]. However, the ADME of the primary psychoactive compound in cannabis, Δ9-tetrahydrocannabinol (THC), is poorly understood. There have been attempts to develop a standardized THC unit to better regulate the industry, yet more insight is needed to ensure the safe usage of cannabis [9].

THC and its primary metabolite, 11-hydroxy-Δ9-tetrahydrocannabinol (11-OH-THC) are psychoactive compounds that can lead to conceptual disorganization, hallucinations, blunted affect, somatic concern, motor retardation and poor attention [10]. As a result, precautions must be taken to ensure that individuals who use cannabis for either medicinal or recreational reasons minimize their risks prior to operating a motor vehicle since motor vehicle collisions (MVCs) are a leading source of preventable morbidity and mortality. In 2012, MVCs, associated injuries, and fatalities attributed to driving under the influence of cannabis (DUIC) resulted in costs of greater than $1 billion in Canada [11]. With the recent legalization, both recreational and therapeutic cannabis use may increase and exacerbate this statistic.

Epidemiological research and driving simulators have established that DUIC is associated with significant increases in collision risk [12–16]. However, important questions remain about how cannabis affects driving behavior, who is most likely to be impaired by the drug, and factors that affect the extent of impairment observed. Initial driving studies have found mixed effects of low-dose cannabis due to variations in the measures of driving impairment [17–19]. More recently, studies with moderate (~8% THC) doses have reported increases in lane weaving characterized by the Standard Deviation in Lateral Position (SDLP) [16,20,21] with decreased driving speed as compensation for the impaired driving [21–24]. Studies have also found decreased steering control [22,24], longer reaction times, and increased headway [21]. It should be noted that a recent study did not find any effects of 12% THC on these measures of simulated driving, but did

see an increase in risk of collisions with a driving simulator [25]. These findings demonstrate that additional research must be conducted to gauge the effects of THC, its rates of metabolism, and investigate the duration of its effects on various individuals.

A number of studies over the past several decades have attempted to determine the pharmacokinetic (PK) parameters of smoked cannabis. For the most part, these studies have used relatively low doses of smoked cannabis (generally below 7%), and tracked blood levels of THC for up to about 8 hours after dosage [26–32]. Doses of THC in recreational cannabis have been steadily increasing over the past few decades, and it is not uncommon to find levels of THC in cannabis that exceed 10% [31]. The cannabis available for legal purchase in the province of Ontario by and large contains over 10% THC, and doses in the range of 22% are also common [31]. Thus, there is a need to study the PK curves of more realistic recreational doses of cannabis as well.

PK models for THC metabolism have been previously been explored, but they are limited in their analysis of whole body, lack ADME information, or are animal models [33–37]. Thus, a more comprehensive whole-body physiologically-based pharmacokinetic (PBPK) model for THC metabolism can better advise on safety when using cannabis [38,39]. In this study, we developed a whole-body PBPK model to track the blood THC concentrations after various dosages, accounting for interindividual variations such as age, sex, body composition, bioavailability, and Drug Metabolizing Enzyme (DME) polymorphisms to better advise on the metabolism of THC and provide useful insights for future public health policies. We also combined this model with a previously developed Ethanol model to gain preliminary insights into their combined effect on driving [40].

3.3 Methods

3.3.1 Model Development

The model we modified to track blood THC concentrations is based on a previously developed PBPK model for ethanol metabolism [40]. The current model breaks down the human body into 14 tissue compartments (consisting of the lung, liver, stomach, small intestines, large intestines, pancreas, spleen, kidney, skin, muscle, adipose, brain, heart, and blood) and 3 lumenal compartments (consisting of the lumen of stomach, small intestines, and large intestines). A schematic of the model can be found in *Figure 3.1*.

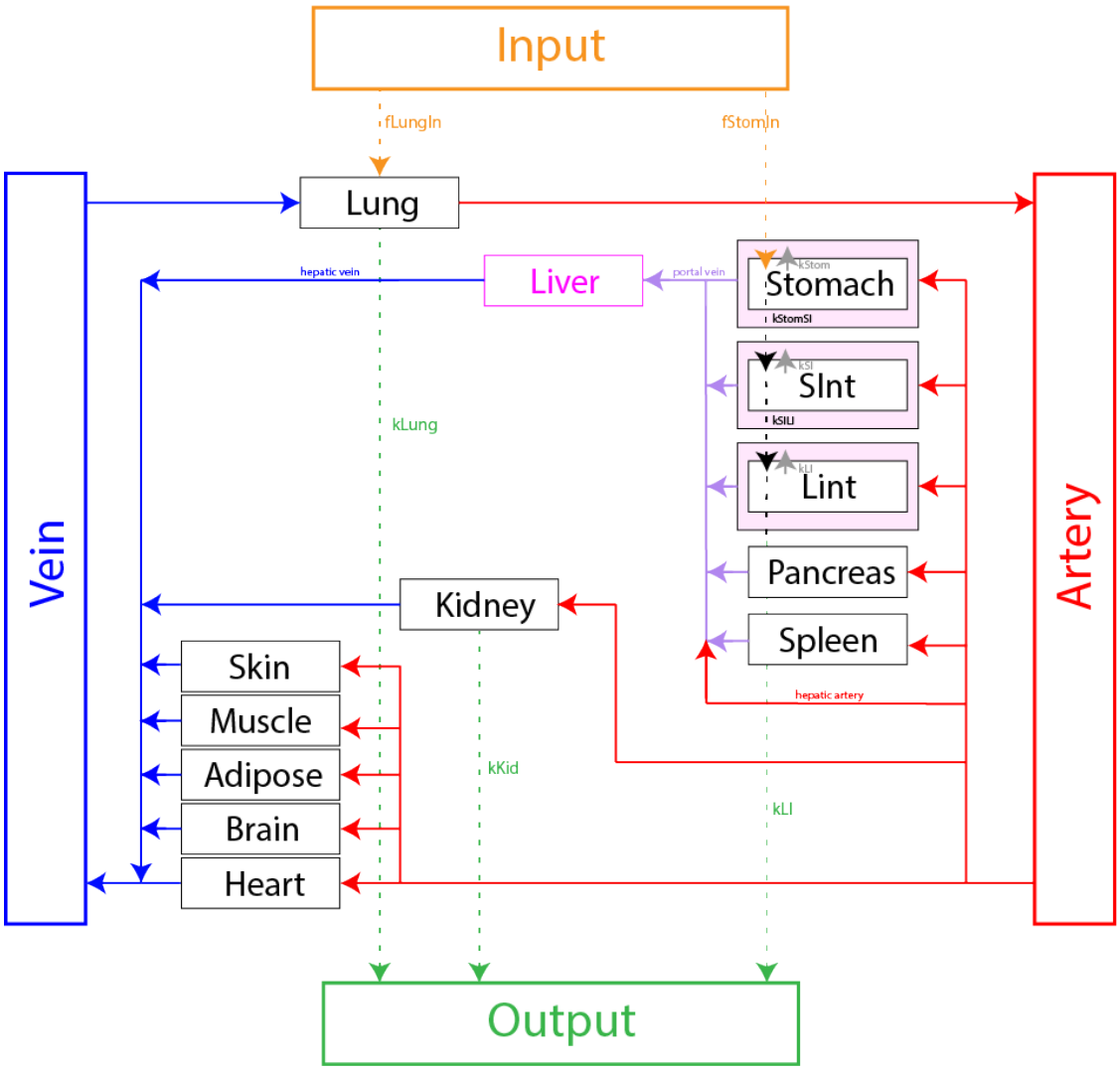

Fig. 3.1 Schematic of the PBPK model. The red, blue, and purple lines denote arterial, venous, and hepatic portal blood flows, respectively. The dashed lines show metabolite inputs and outputs. There are two mixing points in the model at the lung and at the liver to account for their respective physiology. SInt and LInt denote the small and large intestines, respectively.

Within the model, an individual's age, sex, height, weight, and body fat percentage are taken as inputs to estimate the mass of the various tissue compartments as well as the blood flow to each organ [41,42]. THC is a highly lipophilic substance, and while it is understood that it prefers to stay in fatty tissue, its distribution in other organs is not well understood. Thus, this model assumes that the partitioning of metabolites between tissue and blood is in equilibrium and thus uses the drug lipophilicity (its ability to dissolve in lipids) and fraction unbound to calculate tissue-partition coefficients based on the tissue proportions of water, neutral lipids, and phospholipids [43–45].

Table 3.1 Pharmacokinetic parameters for THC

Parameter	Value	Unit
Molecular Weight	314.45	g/mol
Lipophilicity (log K_{ow})	5.648	
Fraction Unbound	0.01	

The model is formulated as a system of ordinary differential equations (ODEs) which represent both the transport of metabolites across the various compartments in the human body such as the organs and blood as well as enzyme activity via Michaelis-Menten kinetics. In *Equations 3.1-3.3*, the development of the ODEs from mass balance is shown. These ODEs characterizing the concentration changes in each organ are solved simultaneously using forward Newton-Raphson numerical integration on MATLAB© (Version 9.6.0.1174912 R2019a, CPU: 2.6 GHz 6-Core Intel Core i7, RAM: 16 GB 2667 MHz DDR4, OS: macOS Catalina 10.15.6) at each time step.

It is established in literature that THC metabolism is governed by liver Cytochrome P450 enzymes, notably CYP2C9 [46]. THC is primarily metabolized by CYP2C9 into 11-OH-THC, which is further metabolized by CYP2C9 into 11-nor-9-carboxy tetrahydrocannabinol (THC-COOH), and finally glucuronidated by UDP-glucuronosyltransferases for renal excretion [47]. Other enzymes such as CYP3A4 [48,49], COMT [50,51], CB1 [52,53] can also contribute and this can be

accounted for in future iterations of the model when kinetic data is more readily available. Within different populations, genetic polymorphisms in CYP2C9 isoforms can lead to varying metabolism rates and therefore overall drug exposure, which is accounted for in the model with different Michaelis-Menten kinetic parameters V_{max} and K_m for the reactions as shown in *Table 3.3* [54].

$$\textbf{accumulation} = \textbf{in} - \textbf{out} + \textbf{generation} - \textbf{consumed} \quad (3.1)$$

$$\Delta\text{concentration} = \text{artery} - \text{vein} - \text{excretion} - \text{metabolized} \quad (3.2)$$

$$\frac{dC_i}{dt} = \frac{Q_i}{V_i}\left(C_{blood} - \frac{C_i}{K_i}\right) - k_i C_i - R_i, \text{where } R_i = \left(\frac{V_{max} C}{V_{max} + K_m}\right)_i \quad (3.3)$$

Table 3.2 Parameters used in model ODE development

Parameter	Definition	Units	Source
C_i	Concentration of THC in organ **i**	mM	Experimental
Q_i	Blood flow rate to organ **i**	L/min	[41]
V_i	Volume of organ **i**	L	[41]
K_i	Tissue:Blood partition coefficient between organ **i** and blood	mM/mM	[43]
k_i	Clearance rate of THC in organ **i**	1/min	Fitted
R_i	Metabolism of THC in organ **i**	mM/min	[54]
V_{max}	V_{max} from Michaelis-Menten Kinetics	mM/min	[54]
K_m	Michaelis-Menten Constant	mM	[54]

Table 3.3 Michaelis-Menten Parameters for CYP2C9 polymorphisms [54]

CYP2C9 isoform	K_m [uM]	V_{max} [uM/min]
CYP2C9.1 (Arg144)	2.13	6.39
CYP2C9.2 (Cys144)	11.10	10.11
CYP2C9.3 (Leu359)	6.69	5.36

In these ODEs, organ blood flow (Q_i) and organ volume (V_i) were physiological parameters calculated by correlations with age, sex, height, weight, and body fat percentage [35]. The tissue partition coefficient (K_i) represents the pharmacokinetic properties of THC in the various compartments and was calculated based on lipophilicity, fraction unbound, and tissue composition [37]. The clearance rate constant (k_i) refers to the first-order elimination of THC from excreting organs such as the kidney, lungs, and large intestinal lumen. R_i refers to any potential reactions that may occur in the tissue. The generic equation for most compartments is shown in *Equation 3.3*. For all of the tissue-specific equations, please refer to the Appendix (7.1.1).

3.3.2 Driving Simulator Calculations

In a study by Hartman et al. to gauge the relative effects of THC and ethanol on driving effects, it was found that the effects of THC and ethanol on the Standard Deviation of Lateral Position (SDLP) were additive rather than synergistic, with each ug of THC per liter of blood contributing 0.26cm to SDLP and each 0.01g ethanol per 210L of breath alcohol concentration contributing 0.42cm to SDLP [20]. Given these correlations, a modified ethanol model from Toroghi et al. was combined with the present THC model to evaluate the contributions of both recreational drugs on the risk of lane departure [40].

3.4 Results & Discussion

3.4.1 Model Fitting with Clinical Data

Given the lack of research on the human pharmacokinetics of THC, the model required the lung elimination parameters (k_{lung}) to be fitted against clinical data for better characterization. Experimental data from Brands 2019 was used to fit the model for k_{lung} (*Figure 3.2a*)[55].

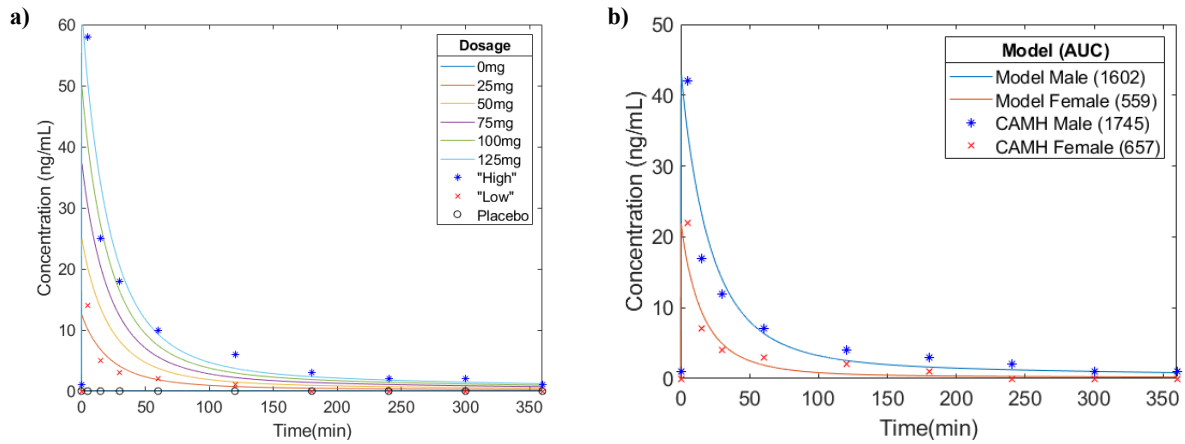

Fig. 3.2 (a) Fitted model with experimental data from Brands et al., 2019 [55]. Different dosages were plotted to correlate "high" and "low" dosages with the best simulated dosages. **(b)** Comparison of the fitted model with male/female data from Matheson et al., 2020 [56]. Area Under the Curve was calculated with trapezoid method with the units ng*min/mL.

In this study, 91 cannabis users aged between 19-25 years old were given a maximum of 10 min to smoke ad libitum either a 750mg 12.5% THC cannabis cigarette or placebo cigarette. Blood THC concentrations, subjective and physiological effects were tracked, and simulated driver behavior measured. Non-placebo participants were divided into "high" and "low" dose groups based on a median split of whole-blood THC concentrations at the time of driving. Using experimental data, we identified the fitting parameters for the lung:blood partition coefficient, K_{lung} (0.0057) and plotted the curves for various concentrations of THC against the experimental data. As demonstrated in *Figure 3.2a*, the "high" group correlated well with a 100mg dose, whereas the "low" group correlated well with a 25mg dose based on Area Under the Curve (AUC) calculations which represent total systemic exposure. The experimental data for the "high" dosage showed an AUC of 2375 ng*ml/min and the fitted model showed an AUC of 2327 ng*ml/min with a Mean Absolute Error (MAE) of 2.4286. The experimental data for the "low" dosage showed an AUC of 385ng*ml/min and the fitted model showed an AUC of 468 ng*ml/min with a MAE of 0.8557.

In a subsequent report by Matheson et al., the data from Brands et al. were further analyzed to provide insights on the impact of sex differences on THC pharmacokinetics. It was found that while females on average smoked less cannabis compared to males and encountered a lower blood THC level, there were no statistically significant differences in subjective effect based on Visual Analogue Scale assessments [56]. We compared our k_{lung} fitted model against this experimental data, with changes in the ODEs to account for the sex-based physiological differences according to the correlations in Stader et al. [41]. In *Figure 3.2b*, we see that the male experimental data had an AUC of 1745 ng*ml/min and the fitted model had an AUC of 1602 ng*ml/min with a MAE of 0.7697. Similarly, the female experimental data had an AUC of 559 ng*ml/min and the fitted model had an AUC of 657 ng*ml/min with a MAE of 0.2123. The similarities in AUC demonstrate that the PBPK model shows similar levels of drug exposure as the clinical studies.

In the following sections, we used the fitted model to make predictions on age, dosage, dosing regimen, bioavailability, and CYP polymorphisms to gain further insight into the pharmacokinetics of THC. Furthermore, we explored the advantages of using a PBPK model as well as integrated the present model with a previously developed ethanol metabolism model to gain insights on the risks of lane departure. Unless otherwise specified, simulation parameters were: sex = male, age = 25, height = 180cm, weight = 70kg, fat = 20%, dosage = 25mg, bioavailability = 0.25, CYP2C9.1 variant.

3.4.2 Fitted Model Simulations

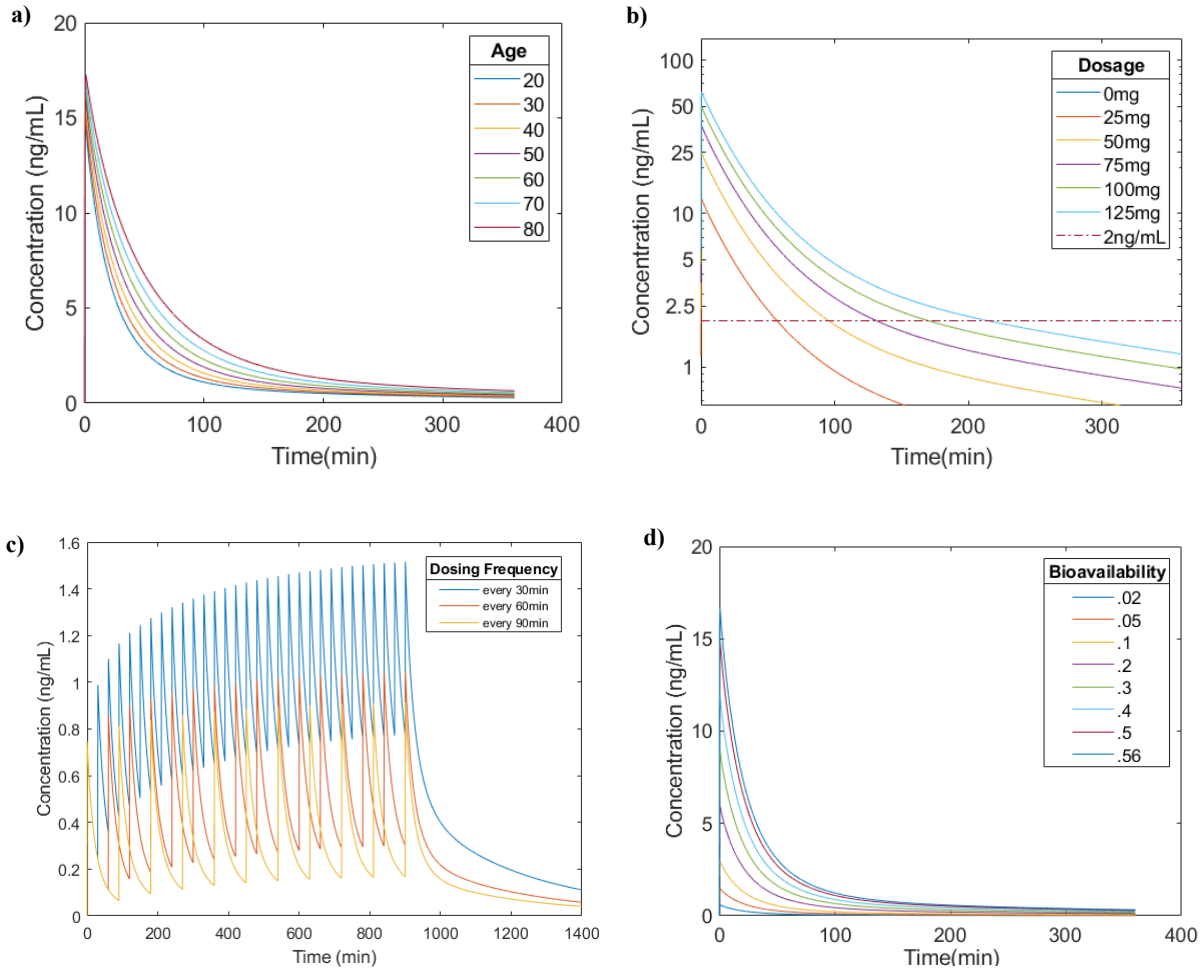

Fig. 3.3 (a) The effect of Age on THC metabolism in males weighing 70kg, height of 180cm, and 20% body fat smoking 25mg of THC at a bioavailability of 0.25 and the CYP2C9.1 variant. All variables were kept constant except for the age of the simulated individual. **(b)** The effect of dosage on the time required to reach the legal limit of 2ng/mL for a male of age 25 weighing 70kg, height of 180cm, and 20% body fat smoking various doses of THC at a bioavailability of 0.25 and the CYP2C9.1 variant. The time to sobriety was calculated with the intersection of the time-concentration curves with the legal limit. **(c)** The effect of dosing regimen and smoking at different time intervals in a male of age 25 weighing 70kg, height of 180cm, and 20% body fat smoking 5mg of THC at a bioavailability of 0.25 and the CYP2C9.1 variant. Different dosing intervals yielded different "steady state" levels of THC in the blood. **(d)** Effect of Bioavailability on THC metabolism. This simulation was done in males weighing 70kg, height of 180cm, and 20% body fat smoking 25mg of THC and the CYP2C9.1 variant. All variables were kept constant except for bioavailability, which ranged from 2-56%.

3.4.3 Increased age leads to slower clearance and higher peak concentration

In *Figure 3.3a*, we see that the maximum THC concentration increases with age, and its clearance rates are reduced. This can be attributed to the reduced cardiac output associated with increased age (See Appendix 7.1.1 for equation), which leads to a slower rate of THC distribution and uptake into organs, especially by the liver which is primarily responsible for metabolism [41]. For individuals who are older, it would be beneficial to have a lesser dosage to maximize safety.

3.4.4 Increasing dosages require longer wait periods to reach sobriety

In *Figure 3.3b*, various doses of THC were explored and the time to reach the legal limit of 2ng/mL were noted. Here, the model predicts that for every 25mg increase in THC intake, the individual must wait an additional 40 minutes prior to driving to ensure that he is under the legal limit. In later experiments we investigate the distribution of THC into the brain and the effect of THC on driving performance to better predict for safety as well. This information could potentially be useful in advising a general rule for THC metabolism, and clinical validation should be applied in the future.

3.4.5 Increased dosing frequency leads to higher steady-state concentrations

In medical settings, there is interest in optimizing dosing regimen to maintain a therapeutic level of THC. In *Figure 3.3c*, we show that multiple 5 mg “standard doses” of THC spaced 30, 60 and 90 minutes apart leads to steady state concentrations of 1.5 ng/mL, 1 ng/mL, and 0.9 ng/mL, respectively. This work can be optimized in the future to assess the effects of different dosing regimen to achieve a desired concentration of THC in the blood.

3.4.6 Increased bioavailability leads to higher peak concentrations and longer clearance times

Bioavailability is defined as the amount of drug that reaches the blood stream from an intake method when compared to an intravenous injection [57]. In a review by Huestis on the human pharmacokinetics of THC, it was found that inhaled THC has a bioavailability of 2-56%, which can account for interindividual differences in blood concentration as well as account for the concentration differences between chronic and occasional users of cannabis [57,58]. Bioavailability is associated with the inhalation technique, and we demonstrate in *Figure 3.3d* that as bioavailability increases, the amount of inhaled THC can vary drastically and alter the shape of the elimination curves. This parameter has large potential for interindividual differences, and should be controlled for future studies.

3.4.7 PBPK Model can allow for analysis of multiple organ compartments

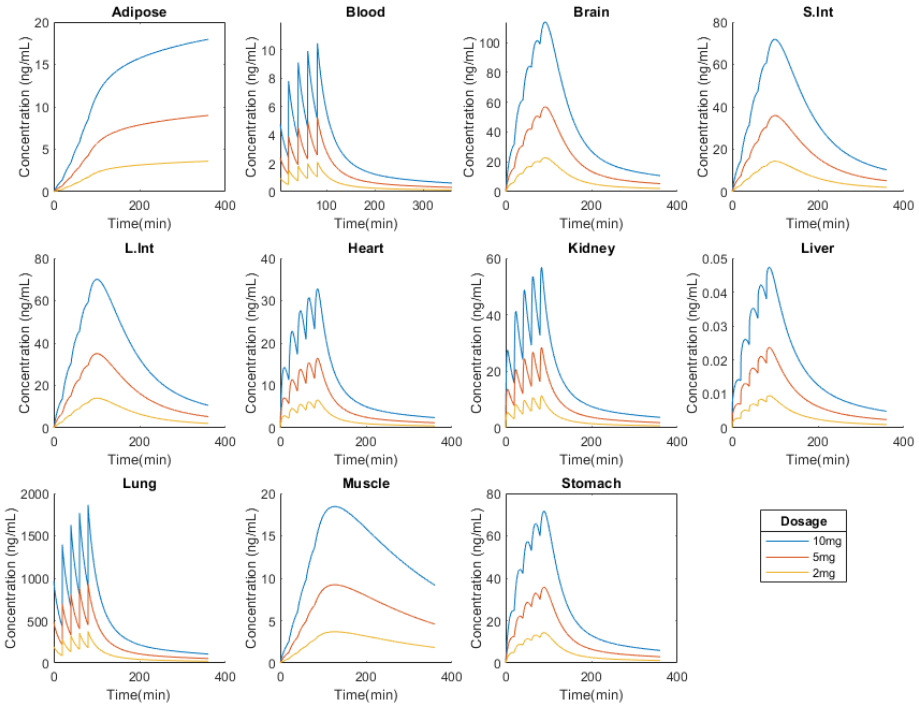

Fig. 3.4 Overview of multi-compartment tracking of THC concentrations. Different dosages were used to visualize the accumulation of THC in various tissues. Simulations were done in males weighing 70kg, height of 180cm, and 20% body fat smoking various doses of THC at a bioavailability of 0.25 and the CYP2C9.1 variant.

Given that the model is able to advise on the concentration of THC in other compartments of the body aside from the clinically measured blood levels, we are able to show in *Figure 3.4* the pharmacodynamics of THC in other physiological components. This can be useful in understanding the potential effects that THC can have in various organs that has not been fully explored or understood yet. For instance, THC may adversely affect male reproductive organs since the endocannabinoid system is involved in spermatogenesis [59]. This is not limited to just the reproductive system as the endocannabinoid system has regulatory effects on other parts of the body, but its effects are not very well understood due to limited research. Interestingly, different organs have different responses to the doses of THC due to their differing compositions. In adipose tissue, we see a slow increase as the lipophilic THC is absorbed and eventually released back to the bloodstream, whereas in the lungs THC is quickly distributed into the bloodstream.

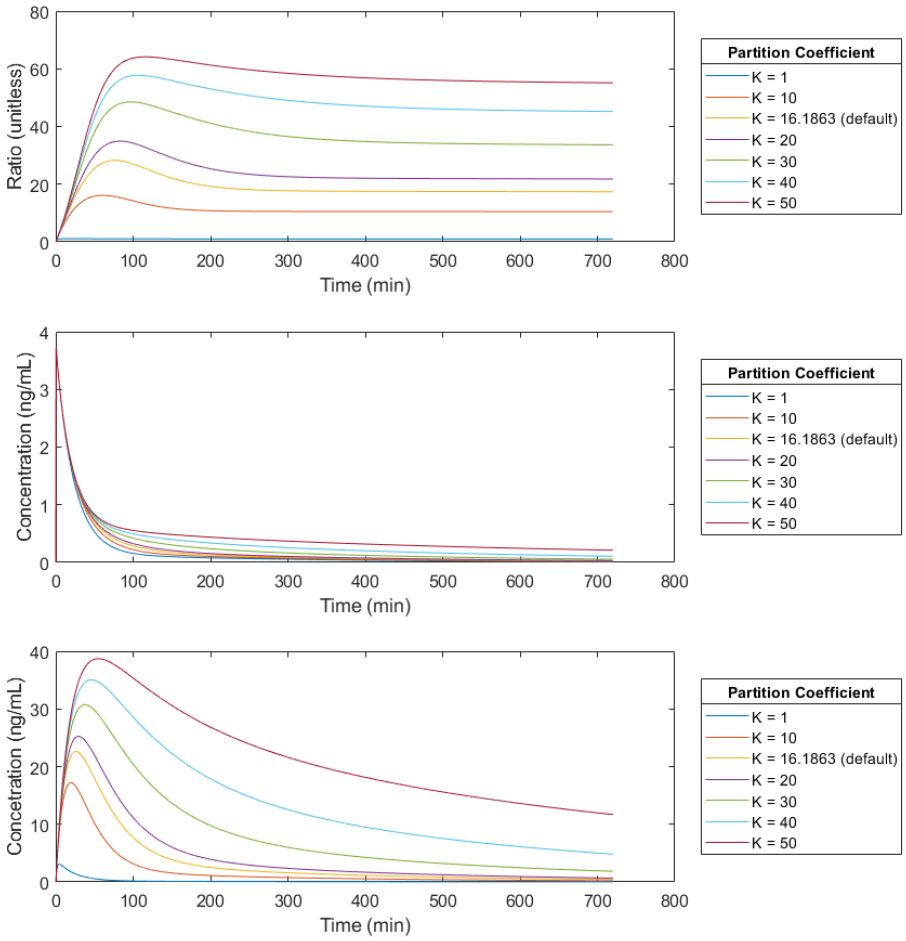

Fig. 3.5 (a) Blood-brain concentration ratio of THC with varying brain:blood partition coefficients (K_{brain}). **(b)** Blood concentration profile of THC for varying partition coefficients. **(c)** Brain concentration profile of THC for varying partition coefficients. Simulations were done in males weighing 70kg, height of 180cm, and 20% body fat smoking various doses of THC at a bioavailability of 0.25 and the CYP2C9.1 variant.

Furthermore, in *Figure 3.5* we characterize the concentration of THC in the brain as well as the ratio of THC concentration in the brain to the THC concentration in the blood. The brain:blood partition coefficient (K_{brain}), which measures how well the brain retains and absorbs THC, was changed to simulate different levels of brain receptor occupancy and receptor kinetics. Different individuals will have different responses to THC due to factors such as genetics or habitual use. For chronic cannabis users, there is a downregulation in cannabinoid receptors in the brain, leading to less uptake by the tissue [60,61]. The simulation above demonstrates how increased tolerance to THC due to habitual usage can be simulated by changing the brain:blood partition coefficient. With increasing partition constant values, it is shown that it takes an increasing

amount of time for THC to be removed from the brain, corresponding to cannabis-naive individuals with lower tolerances. Conversely, lower brain:blood partition coefficients result in a quicker clearance of THC from the brain, which can simulate individuals that have a higher tolerance to THC. In the future, receptor kinetics characterizing the interactions between THC and CB1 receptors could be incorporated to better demonstrate the psychoactive effects of THC.

3.4.8 CYP2C9 Polymorphism Simulations

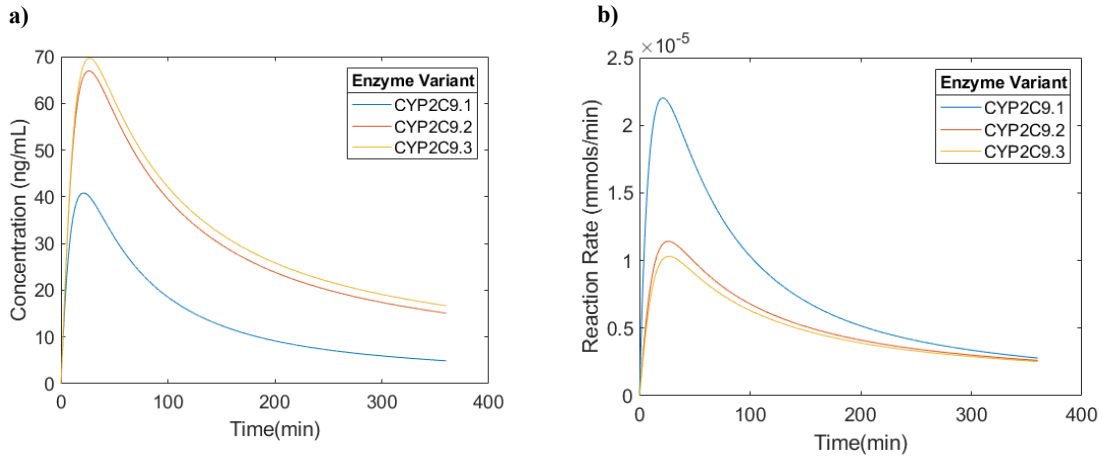

Fig. 3.6 (a) The effect of CYP2C9 polymorphisms on the metabolism of THC, and **(b)** the reaction rates of CYP2C9 isoforms. The simulations were done in males weighing 70kg, height of 180cm, and 20% body fat smoking 25mg of THC at a bioavailability of 0.25. All variables were kept constant except for the Michaelis-Menten parameters of K_m and V_{max}. **(b)** The various metabolism rates of the enzyme variants over time were tracked as well.

The CYP2C9.2 and CYP2C9.3 variants have been implicated in a 30% decrease in THC clearance rates in initial findings by Tina Bland et al. 2015 [54]. In *Figure 3.6b*, we find that the maximum metabolism rate of CYP2C9.1 is approximately double that of the other isoforms. This leads to the large change in THC exposure and peak concentrations, as shown by the data in *Table 3.4*. We see that for the same dosage, CYP2C9.2 and CYP2C9.3 have slower rates of metabolism and a higher peak concentration, which could be a plausible explanation for why certain populations are more susceptible to the effects of THC.

Table 3.4 Results of CYP2C9 Polymorphism Simulations

CYP2C9 Polymorphism	Area Under the Curve (ng*min/mL)	Maximum Concentration (ng/mL)
CYP2C9.1	5240.5	40.81
CYP2C9.2	11167.9	66.94
CYP2C9.3	11920.8	69.64

3.4.9 Combined Model Simulations

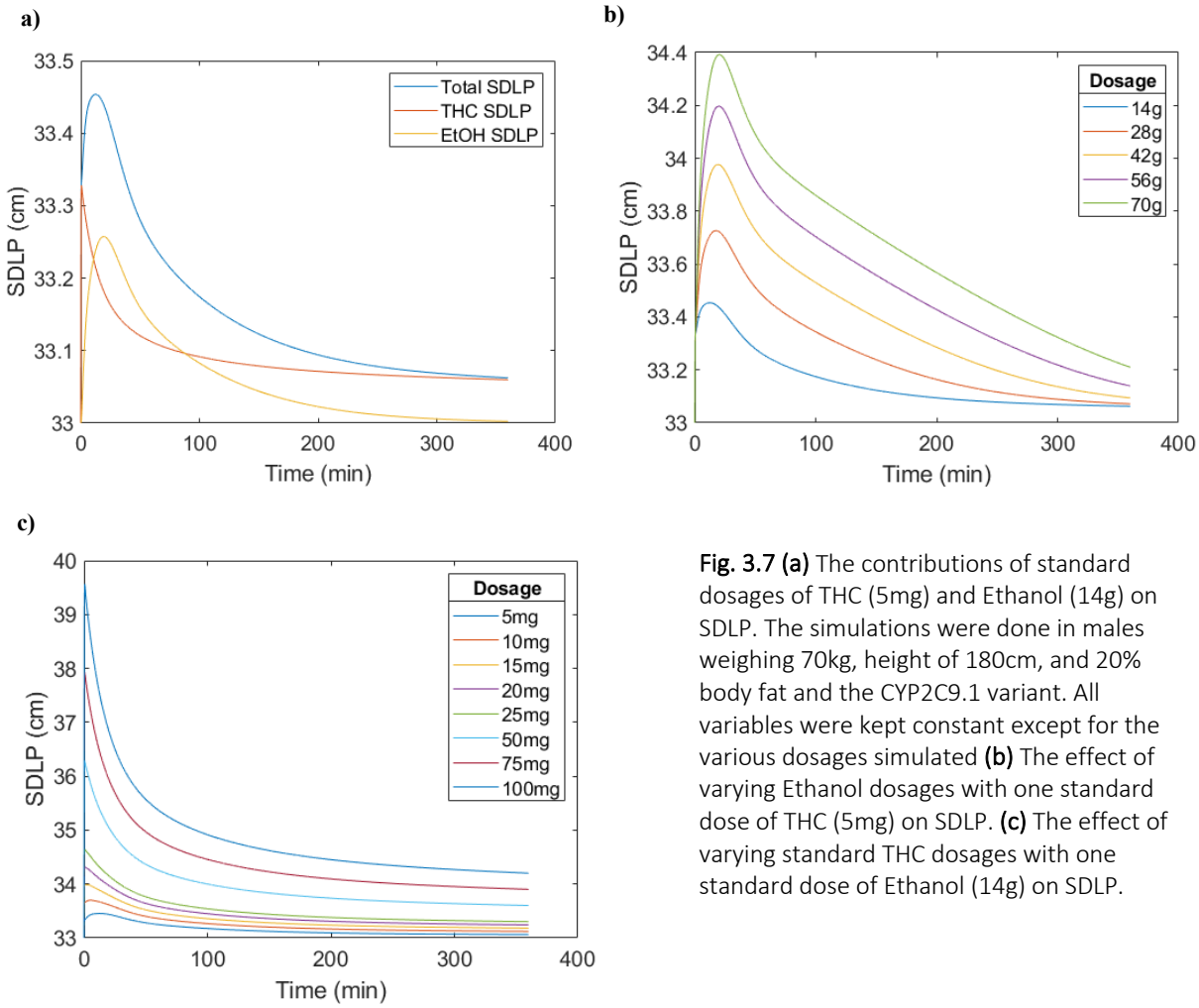

Fig. 3.7 (a) The contributions of standard dosages of THC (5mg) and Ethanol (14g) on SDLP. The simulations were done in males weighing 70kg, height of 180cm, and 20% body fat and the CYP2C9.1 variant. All variables were kept constant except for the various dosages simulated **(b)** The effect of varying Ethanol dosages with one standard dose of THC (5mg) on SDLP. **(c)** The effect of varying standard THC dosages with one standard dose of Ethanol (14g) on SDLP.

Lastly, the results of this model were combined with the previously developed ethanol model to gauge the effect of both THC and ethanol on driving [40]. In *Figure 3.7a*, we see that standard doses of both drugs result in similar magnitudes of changes in SDLP. Since ethanol is absorbed through the stomach and takes more time, we see the effects of THC on SDLP first, followed by an increase of SDLP as ethanol is absorbed. However, due to ethanol's faster metabolism rate, the ethanol SDLP effects quickly subside, resulting in only the residual effects from THC afterwards. In *Figures 3.7b* and *Figure3.7c*, we compare the effects of various ethanol and THC dosages and see a similar effect - higher doses of THC have longer lasting small residual effects on SDLP, while higher doses of ethanol have a significant acute effect. Future studies could investigate the acceptable ranges of SDLP for minimizing lane departure, and update guidelines for legal blood concentrations of both drugs.

3.4.10 Model Limitations

Some limitations of the model include the following:

The Michaelis-Menten parameters were derived from *in vitro* data, whereas the simulations mimicked human experiments. The actual V_{max} and K_m could potentially be different and impact the metabolic rates of the different enzyme isoforms. One recent study showed that the isoforms do not make a large difference in the concentrations, and thus future studies should investigate this relationship further [62].

The organ partition coefficients were calculated based on the molecular lipophilicity and fraction unbound, and does not take into account possible transport mechanisms. In the future, this can be remedied by studying the partitioning with tissue samples for more accurate analyses.

Enzymes other than CYP2C9 are involved in the metabolism of THC, and more information can be included in future iterations when their kinetic parameters are better understood. Furthermore, metabolites of THC (notable the psychoactive 11-OH-THC) can be tracked as well to better predict the impact of cannabis usage on driving ability.

3.5 Conclusion

In this study we have developed a PBPK model for THC metabolism that can allow for insights into the distribution of THC into organs beyond the clinically measured blood concentrations. The model was fitted and validated with clinical data based on sex and dosage, and predictions were made for the effects of sex, dosage, dosing regimen, bioavailability, and CYP variations. Also, the model was able to predict the combined effect of using ethanol and cannabis on the risk of lane departure while driving. The results of these simulations can be used to better predict the effects of a "standard THC unit" on cannabinoid metabolism and help to establish a general rule for safe cannabis usage.

Furthermore, this model establishes a framework for future studies to examine the effects of tolerance, inhalation technique, and subjective effects through the parameters of bioavailability, tissue:blood partition coefficients, and the opportunity to incorporate receptor kinetics when data is more readily available. The work on genetic polymorphisms can advise on using a more personalized medicine approach to future prescriptions of medical cannabis, and can have important implications for the forensic sciences as well. Although this study primarily looks at the metabolism of THC, it is worth noting that the primary metabolite of THC, 11-OH-THC is also psychoactive, and its effects should be explored in future work as well. Different methods of THC dosing including oral or vaping could be investigated with this model, as well as other enzymes that could also contribute to metabolism [46]. Because CYP enzymes are inducible, it is worth investigating the effects of their activation and deactivation as well. Furthermore, since CYP2C9 is also responsible for the metabolism of warfarin and phenytoin, it is worth noting the effects of substrate inhibition of the enzyme as well by incorporating inhibition into the Michaelis-Menten kinetics. In the future, we also plan to test the model against individual time-concentration curves for improved personalization. In conclusion, we have developed a framework of THC metabolism that can be further expanded to better understand the effects of cannabis and advise on public health policies.

3.6 References

Citations formatted in accordance with the Journal of Clinical Pharmacokinetics

1. Holford NHG. Clinical Pharmacokinetics of Ethanol. Clin Pharmacokinet [Internet]. 1987;13:273–92. Available from: http://link.springer.com/10.2165/00003088-198713050-00001
2. Crabb DW, Bosron WF, Li TK. Ethanol metabolism. Pharmacol Ther [Internet]. 1987;34:59–73. Available from: http://www.ncbi.nlm.nih.gov/pubmed/3310044
3. Jones AW, Hahn RG, Stalberg HP. Pharmacokinetics of ethanol in plasma and whole blood: estimation of total body water by the dilution principle. Eur J Clin Pharmacol [Internet]. 1992;42:445–8. Available from: http://www.ncbi.nlm.nih.gov/pubmed/1516610
4. Zhang Y, Wu C, Wan J. Development and validation of a model to predict blood alcohol concentrations: Updating the NHTSA equation. Addict Behav [Internet]. Elsevier Ltd; 2017;71:46–53. Available from: http://dx.doi.org/10.1016/j.addbeh.2017.02.022
5. Jones AW. Alcohol, its absorption, distribution, metabolism, and excretion in the body and pharmacokinetic calculations. Wiley Interdiscip Rev Forensic Sci [Internet]. 2019;1:1–26. Available from: https://onlinelibrary.wiley.com/doi/abs/10.1002/wfs2.1340
6. MADD The ABCs of BACs [Internet]. 2014 [cited 2020 Sep 8]. p. 1–8. Available from: https://www.madd.ca/media/docs/ABCs _of_BACs_FINALdoc.pdf
7. Centre for Addiction and Mental Health. Do You Know.. Alcohol and Other Drugs and Driving [Internet]. 2020 [cited 2020 Sep 8]. Available from: https://www.camh.ca/en/health-info/guides-and-publications/alcohol-and-other-drugs-and-driving
8. Scott-Parker B, Stokes L, Panaho S, Cawkwell M, Caldwell J. Are you okay to drive? Commuting behavior and blood alcohol concentrations among restaurant diners. Traffic Inj Prev [Internet]. Taylor & Francis; 2017;18:673–80. Available from: https://doi.org/10.1080/15389588.2017.1293824
9. Freeman TP, Lorenzetti V. 'Standard THC units': a proposal to standardize dose across all cannabis products and methods of administration. Addiction [Internet]. 2020;115:1207–16. Available from: https://onlinelibrary.wiley.com/doi/abs/10.1111/add.14842
10. Ganesh S, Cortes-Briones J, Ranganathan M, Radhakrishnan R, Skosnik PD, D'Souza DC. Psychosis-Relevant Effects of Intravenous Delta-9-Tetrahydrocannabinol: A Mega Analysis of Individual Participant-Data from Human Laboratory Studies. Int J Neuropsychopharmacol [Internet]. 2020;0:1–33. Available from: https://academic.oup.com/ijnp/advance-article/doi/10.1093/ijnp/pyaa031/5834890
11. Wettlaufer A, Florica RO, Asbridge M, Beirness D, Brubacher J, Callaghan R, et al. Estimating the harms and costs of cannabis-attributable collisions in the Canadian provinces. Drug Alcohol Depend [Internet]. 2017;173:185–90. Available from: http://www.sciencedirect.com/science/article/pii/S0376871617300686
12. Asbridge M, Hayden JA, Cartwright JL. Acute cannabis consumption and motor vehicle collision risk: systematic review of observational studies and meta-analysis. BMJ [Internet]. 2012;344:e536. Available from: http://www.ncbi.nlm.nih.gov/pubmed/22323502
13. Asbridge M, Mann R, Cusimano MD, Trayling C, Roerecke M, Tallon JM, et al. Cannabis and traffic collision risk: findings from a case-crossover study of injured drivers presenting to emergency departments. Int J Public Health [Internet]. 2014;59:395–404. Available from: http://link.springer.com/10.1007/s00038-013-0512-z

14. Li M-C, Brady JE, DiMaggio CJ, Lusardi AR, Tzong KY, Li G. Marijuana use and motor vehicle crashes. Epidemiol Rev [Internet]. 2012;34:65–72. Available from: http://www.ncbi.nlm.nih.gov/pubmed/21976636
15. Rogeberg O, Elvik R, White M. Correction to: 'The effects of cannabis intoxication on motor vehicle collision revisited and revised' (2016). Addiction [Internet]. 2018;113:967–9. Available from: http://doi.wiley.com/10.1111/add.14140
16. Micallef J, Dupouey J, Jouve E, Truillet R, Lacarelle B, Taillard J, et al. Cannabis smoking impairs driving performance on the simulator and real driving: a randomized, double-blind, placebo-controlled, crossover trial. Fundam Clin Pharmacol. 2018;32:558–70.
17. Hartman RL, Huestis MA. Cannabis effects on driving skills. Clin Chem. 2013;59:478–92.
18. Ogden EJD, Moskowitz H. Effects of alcohol and other drugs on driver performance. Traffic Inj Prev [Internet]. 2004;5:185–98. Available from: http://www.tandfonline.com/doi/abs/10.1080/15389580490465201
19. Gjerde H, Strand MC, Mørland J. Driving Under the Influence of Non-Alcohol Drugs--An Update Part I: Epidemiological Studies. Forensic Sci Rev [Internet]. 2015;27:89–113. Available from: www.forensicsciencereview.com
20. Hartman RL, Brown TL, Milavetz G, Spurgin A, Pierce RS, Gorelick DA, et al. Cannabis effects on driving lateral control with and without alcohol. Drug Alcohol Depend [Internet]. 2015;154:25–37. Available from: http://www.ncbi.nlm.nih.gov/pubmed/26144593
21. Lenné MG, Dietze PM, Triggs TJ, Walmsley S, Murphy B, Redman JR. The effects of cannabis and alcohol on simulated arterial driving: Influences of driving experience and task demand. Accid Anal Prev [Internet]. 2010;42:859–66. Available from: https://linkinghub.elsevier.com/retrieve/pii/S0001457509000918
22. Ronen A, Gershon P, Drobiner H, Rabinovich A, Bar-Hamburger R, Mechoulam R, et al. Effects of THC on driving performance, physiological state and subjective feelings relative to alcohol. Accid Anal Prev. 2008;
23. Anderson BM, Rizzo M, Block RI, Pearlson GD, O'Leary DS. Sex differences in the effects of marijuana on simulated driving performance. J Psychoactive Drugs. 2010;42:19–30.
24. Ronen A, Chassidim HS, Gershon P, Parmet Y, Rabinovich A, Bar-Hamburger R, et al. The effect of alcohol, THC and their combination on perceived effects, willingness to drive and performance of driving and non-driving tasks. Accid Anal Prev [Internet]. 2010;42:1855–65. Available from: http://www.sciencedirect.com/science/article/pii/S0001457510001429
25. Ogourtsova T, Kalaba M, Gelinas I, Korner-Bitensky N, Ware MA. Cannabis use and driving-related performance in young recreational users: a within-subject randomized clinical trial. C Open. 2018;6:E453–62.
26. Azorlosa JL, Heishman SJ, Stitzer ML, Mahaffey JM. Marijuana smoking: Effect of varying Δ9-tetrahydrocannabinol content and number of puffs. J Pharmacol Exp Ther. 1992;261:114–22.
27. Cone EJ, Huestis MA. Relating Blood Concentrations of Tetrahydrocannabinol and Metabolites to Pharmacologic Effects and Time of Marijuana Usage. Ther Drug Monit [Internet]. 1993;15:527–32. Available from: http://journals.lww.com/00007691-199312000-00013
28. Cooper ZD, Haney M. Comparison of subjective, pharmacokinetic, and physiological effects of marijuana smoked as joints and blunts. Drug Alcohol Depend [Internet]. 2009;103:107–13. Available from: http://www.sciencedirect.com/science/article/pii/S0376871609001045
29. Heishman SJ, Huestis MA, Henningfield JE, Cone EJ. Acute and residual effects of marijuana: Profiles of plasma THC levels, physiological, subjective, and performance measures. Pharmacol

Biochem Behav [Internet]. 1990;37:561–5. Available from: http://www.ncbi.nlm.nih.gov/pubmed/1965045
30. Huestis MA, Cone EJ. Relationship of 9-Tetrahydrocannabinol Concentrations in Oral Fluid and Plasma after Controlled Administration of Smoked Cannabis. J Anal Toxicol [Internet]. 2004;28:394–9. Available from: https://academic.oup.com/jat/article-lookup/doi/10.1093/jat/28.6.394
31. Lee D, Bergamaschi MM, Milman G, Barnes AJ, Queiroz RHC, Vandrey R, et al. Plasma Cannabinoid Pharmacokinetics After Controlled Smoking and Ad libitum Cannabis Smoking in Chronic Frequent Users. J Anal Toxicol [Internet]. 2015;39:580–7. Available from: https://pubmed.ncbi.nlm.nih.gov/26378131/
32. Brenneisen R, Meyer P, Chtioui H, Saugy M, Kamber M. Plasma and urine profiles of Δ9-tetrahydrocannabinol and its metabolites 11-hydroxy-Δ9-tetrahydrocannabinol and 11-nor-9-carboxy-Δ9-tetrahydrocannabinol after cannabis smoking by male volunteers to estimate recent consumption by athletes. Anal Bioanal Chem [Internet]. 2010;396:2493–502. Available from: https://pubmed.ncbi.nlm.nih.gov/20112012/
33. Marsot A, Audebert C, Attolini L, Lacarelle B, Micallef J, Blin O. Population pharmacokinetics model of THC used by pulmonary route in occasional cannabis smokers. J Pharmacol Toxicol Methods [Internet]. Elsevier Inc.; 2017;85:49–54. Available from: http://dx.doi.org/10.1016/j.vascn.2017.02.003
34. Heuberger JAAC, Guan Z, Oyetayo OO, Klumpers L, Morrison PD, Beumer TL, et al. Population Pharmacokinetic Model of THC Integrates Oral, Intravenous, and Pulmonary Dosing and Characterizes Short- and Long-term Pharmacokinetics. Clin Pharmacokinet. 2015;54:209–19.
35. Wolowich WR, Greif R, Kleine-Brueggeney M, Bernhard W, Theiler L. Minimal Physiologically Based Pharmacokinetic Model of Intravenously and Orally Administered Delta-9-Tetrahydrocannabinol in Healthy Volunteers. Eur J Drug Metab Pharmacokinet [Internet]. Springer International Publishing; 2019;44:691–711. Available from: https://doi.org/10.1007/s13318-019-00559-7
36. Methaneethorn J, Naosang K, Kaewworasut P, Poomsaidorn C, Lohitnavy M. Development of a Physiologically-Based Pharmacokinetic Model of Δ9-Tetrahydrocannabinol in Mice, Rats, and Pigs. Eur J Drug Metab Pharmacokinet [Internet]. 2020;45:487–94. Available from: http://link.springer.com/10.1007/s13318-020-00616-6
37. Awasthi R, An G, Donovan MD, Boles Ponto LL. Relating Observed Psychoactive Effects to the Plasma Concentrations of Delta-9-Tetrahydrocannabinol and Its Active Metabolite: An Effect-Compartment Modeling Approach. J Pharm Sci [Internet]. 2018;107:745–55. Available from: https://jpharmsci.org/article/S0022-3549(17)30632-9/fulltext#
38. Ginsburg BC. Toward a Comprehensive Model of Δ9-Tetrahydrocannabinol Pharmacokinetics Using a Population Pharmacokinetics Approach. Clin Pharmacokinet [Internet]. 2015;54:129–31. Available from: http://link.springer.com/10.1007/s40262-014-0210-x
39. MacCallum CA, Russo EB. Practical considerations in medical cannabis administration and dosing. Eur J Intern Med [Internet]. 2018;49:12–9. Available from: https://linkinghub.elsevier.com/retrieve/pii/S0953620518300049
40. Toroghi MK, Cluett WR, Mahadevan R. Multiscale Metabolic Modeling Approach for Predicting Blood Alcohol Concentration. IEEE Life Sci Lett. 2017;2:59–62.
41. Stader F, Penny MA, Siccardi M, Marzolini C. A Comprehensive Framework for Physiologically-Based Pharmacokinetic Modeling in Matlab. CPT Pharmacometrics Syst

Pharmacol [Internet]. 2019;psp4.12399. Available from: https://ascpt.onlinelibrary.wiley.com/doi/abs/10.1002/psp4.12399
42. Brown RP, Delp MD, Lindstedt SL, Rhomberg LR, Beliles RP. PHYSIOLOGICALLY BASED PHARMACOKINETIC MODELS Protection Agency ; V. Toxicol Ind Health. 1997;13:407–84.
43. Poulin P, Schoenlein K, Theil FP. Prediction of adipose tissue: Plasma partition coefficients for structurally unrelated drugs. J Pharm Sci. 2001;90:436–47.
44. Peters SA. Physiologically-Based Pharmacokinetic (PBPK) Modeling and Simulations [Internet]. Physiol. Pharmacokinet. Model. Simulations Princ. Methods, Appl. Pharm. Ind. Hoboken, NJ, USA: John Wiley & Sons, Inc.; 2012. Available from: http://doi.wiley.com/10.1002/9781118140291
45. Bansal S, Maharao N, Paine MF, Unadkat JD. Predicting the potential for cannabinoids to precipitate pharmacokinetic drug interactions via reversible inhibition or inactivation of major cytochromes P450. Drug Metab Dispos [Internet]. 2020;DMD-AR-2020-000073. Available from: http://dmd.aspetjournals.org/lookup/doi/10.1124/dmd.120.000073
46. Watanabe K, Yamaori S, Funahashi T, Kimura T, Yamamoto I. Cytochrome P450 enzymes involved in the metabolism of tetrahydrocannabinols and cannabinol by human hepatic microsomes. Life Sci [Internet]. 2007;80:1415–9. Available from: https://linkinghub.elsevier.com/retrieve/pii/S0024320507000495
47. Mazur A, Lichti CF, Prather PL, Zielinska AK, Bratton SM, Gallus-Zawada A, et al. Characterization of human hepatic and extrahepatic UDP-glucuronosyltransferase enzymes involved in the metabolism of classic cannabinoids. Drug Metab Dispos [Internet]. 2009;37:1496–504. Available from: http://dmd.aspetjournals.org/lookup/doi/10.1124/dmd.109.026898
48. Anderson GD, Chan L-N. Pharmacokinetic Drug Interactions with Tobacco, Cannabinoids and Smoking Cessation Products. Clin Pharmacokinet. Springer International Publishing; 2016;55:1353–68.
49. Jiang R, Yamaori S, Takeda S, Yamamoto I, Watanabe K. Identification of cytochrome P450 enzymes responsible for metabolism of cannabidiol by human liver microsomes. Life Sci [Internet]. Elsevier Inc.; 2011;89:165–70. Available from: http://dx.doi.org/10.1016/j.lfs.2011.05.018
50. Ranganathan M, De Aquino JP, Cortes-Briones JA, Radhakrishnan R, Pittman B, Bhakta S, et al. Highs and lows of cannabinoid-dopamine interactions: effects of genetic variability and pharmacological modulation of catechol-O-methyl transferase on the acute response to delta-9-tetrahydrocannabinol in humans. Psychopharmacology (Berl) [Internet]. Psychopharmacology; 2019;236:3209–19. Available from: http://www.ncbi.nlm.nih.gov/pubmed/31187152
51. Sherif M, Radhakrishnan R, D'Souza DC, Ranganathan M. Human Laboratory Studies on Cannabinoids and Psychosis. Biol Psychiatry [Internet]. Elsevier; 2016;79:526–38. Available from: http://dx.doi.org/10.1016/j.biopsych.2016.01.011
52. Hayakawa K, Mishima K, Hazekawa M, Sano K, Irie K, Orito K, et al. Cannabidiol potentiates pharmacological effects of Delta(9)-tetrahydrocannabinol via CB(1) receptor-dependent mechanism. Brain Res [Internet]. 2008;1188:157–64. Available from: http://www.ncbi.nlm.nih.gov/pubmed/18021759
53. Viñals X, Moreno E, Lanfumey L, Cordomí A, Pastor A, de La Torre R, et al. Cognitive Impairment Induced by Delta9-tetrahydrocannabinol Occurs through Heteromers between Cannabinoid CB1 and Serotonin 5-HT2A Receptors. PLoS Biol [Internet]. 2015;13:e1002194.

Available from: http://www.ncbi.nlm.nih.gov/pubmed/26158621
54. Bland TM, Haining RL, Tracy TS, Callery PS. CYP2C-catalyzed delta(9)-tetrahydrocannabinol metabolism: Kinetics, pharmacogenetics and interaction with phenytoin. Biochem Pharmacol. 2005;70:1096–103.
55. Brands B, Mann RE, Wickens CM, Sproule B, Stoduto G, Sayer GS, et al. Acute and residual effects of smoked cannabis: Impact on driving speed and lateral control, heart rate, and self-reported drug effects. Drug Alcohol Depend [Internet]. Elsevier; 2019;205:107641. Available from: https://doi.org/10.1016/j.drugalcdep.2019.107641
56. Matheson J, Sproule B, Di Ciano P, Fares A, Le Foll B, Mann RE, et al. Sex differences in the acute effects of smoked cannabis: evidence from a human laboratory study of young adults. Psychopharmacology (Berl) [Internet]. 2020;237:305–16. Available from: http://link.springer.com/10.1007/s00213-019-05369-y
57. Huestis MA. Human cannabinoid pharmacokinetics. Chem Biodivers. 2007;4:1770–804.
58. Hartley S, Simon N, Larabi A, Vaugier I, Barbot F, Quera-Salva MA, et al. Effect of smoked cannabis on vigilance and accident risk using simulated driving in occasional and chronic users and the pharmacokinetic-pharmacodynamic relationship. Clin Chem. 2019;65:684–93.
59. López-Cardona AP, Ibarra-Lecue I, Laguna-Barraza R, Pérez-Cerezales S, Urigüen L, Agirregoitia N, et al. Effect of chronic THC administration in the reproductive organs of male mice, spermatozoa and in vitro fertilization. Biochem Pharmacol [Internet]. Elsevier; 2018;157:294–303. Available from: https://doi.org/10.1016/j.bcp.2018.07.045
60. Ludanyi A, Eross L, Czirjak S, Vajda J, Halasz P, Watanabe M, et al. Downregulation of the CB1 Cannabinoid Receptor and Related Molecular Elements of the Endocannabinoid System in Epileptic Human Hippocampus. J Neurosci [Internet]. 2008;28:2976–90. Available from: http://www.jneurosci.org/content/28/12/2976.abstract
61. D'Souza DC, Cortes-Briones JA, Ranganathan M, Thurnauer H, Creatura G, Surti T, et al. Rapid Changes in Cannabinoid 1 Receptor Availability in Cannabis-Dependent Male Subjects After Abstinence From Cannabis. Biol Psychiatry Cogn Neurosci Neuroimaging [Internet]. Elsevier; 2016;1:60–7. Available from: http://dx.doi.org/10.1016/j.bpsc.2015.09.008
62. Gasse A, Vennemann M, Köhler H, Schürenkamp J. Toxicogenetic analysis of Δ9-THC-metabolizing enzymes. Int J Legal Med [Internet]. International Journal of Legal Medicine; 2020; Available from: http://link.springer.com/10.1007/s00414-020-02380-3

4 Integration of a Physiologically-Based Pharmacokinetic Model with a Whole-Body Genome-Scale Model for Characterization of Ethanol and Acetaldehyde Metabolism

4.1 Abstract

Ethanol is one of the most widely used recreational substances in the world and due to its ubiquitous use, ethanol abuse has been the cause of over 3.3 million deaths each year. In addition to its effects, ethanol's primary metabolite, acetaldehyde, is a carcinogen that can cause symptoms of facial flushing, headaches and nausea. How strongly ethanol or acetaldehyde affects an individual depends highly on the genetic polymorphisms of certain genes. In particular, the genetic polymorphisms of mitochondrial aldehyde dehydrogenase, ALDH2, play a large role in the metabolism of acetaldehyde. Thus, it is important to characterize how genetic variations can lead to different exposures and responses to ethanol and acetaldehyde, and one method is through understanding the pharmacokinetics of ethanol and acetaldehyde.

While the pharmacokinetics of ethanol have been thoroughly explored in previous studies, in this paper we combine a base physiologically-based pharmacokinetic (PBPK) model with a whole-body genome scale model (GEM) to gain further insight into the role of individual variations in ethanol metabolism. This combined model was fit to clinical data and used to show the effect of alcohol concentrations, organ damage, ALDH2 enzyme polymorphisms, and ALDH2-inhibiting drug disulfiram on ethanol and acetaldehyde exposure. The GEM was used to demonstrate that as liver function decreases, other methods of ethanol elimination not traditionally characterized in PBPK models would increase to compensate. Additionally, the model was able to demonstrate that acetaldehyde exposure increases with dosages of disulfiram and decreasing ALDH2 efficiency. Furthermore, moderate consumption rates of ethanol can lead to unexpected accumulations in acetaldehyde. This model combines PBPK modelling with GEM integration to make accurate predictions of metabolism and transform the field of precision medicine.

4.2 Introduction

Ethanol is a drug that has been extensively studied and is widely used in the world today. Ethanol abuse can lead to dependence, liver cirrhosis, social withdrawal, and serious implications when driving under the influence, leading to approximately 3.3 million deaths each year [1]. This alarming number has encouraged researchers to develop mathematical models to better understand ethanol metabolism [2]. It is understood that ethanol is primarily metabolized by liver alcohol dehydrogenase (ADH) along with other enzymes into acetaldehyde, which is in turn primarily eliminated by mitochondrial aldehyde dehydrogenase (ALDH2) into acetate [3-4]. Other processes involved in alcohol metabolism include microsomal ethanol oxidizing systems (namely cytochrome P450 enzyme 2E1), catalase, peroxisomes, and non-oxidative methods such as conversion by fatty acid ethyl esters [3-6].

Acetaldehyde is a toxic metabolite, the buildup of which can cause facial flushing, headaches, nausea, dizziness, and tachycardia [7]. The efficacy of its elimination by ALDH2 is heavily influenced by genetic polymorphisms, and notably East Asian populations with the ALDH2.2 genotypes have almost no ALDH2 activity when compared to the wild type, allowing acetaldehyde to accumulate and cause "flushing" symptoms to occur [8-11]. Interestingly, Disulfiram (Antabuse) and other drugs aimed at reducing alcohol dependence purposefully inhibit ALDH2 to produce the same symptoms and cause oversensitivity to ethanol [12-15]. Acetaldehyde exposure has been implicated in increased risk for a variety of cancers [16-19], and may be involved in alcohol hangovers [20-23]. Thus, it is important to characterize how different populations' genetic variations lead to various exposure and responses to ethanol and acetaldehyde.

The pharmacokinetics of ethanol have been well characterized in literature since Widmark's research in 1933 assuming 0th order elimination [24]. This work was expanded upon by Lundquist and Wolthers, who incorporated Michaelis-Menten Kinetics to describe the non-linearity of elimination curves below 0.2mg/mL [25]. In the late 1900s, further research on ethanol metabolism investigated the distribution of ethanol in the blood proportional to total

body water, the effect of first-pass metabolism by the stomach, and extrahepatic pathways for ethanol clearance [26-31]. This work continues today in the form of physiologically-based pharmacokinetic (PBPK) models, one of which we have previously developed. We used this model to capture the effect of different metabolic mechanisms, aging, biochemical variation in enzyme activity, sex differences, and the "meal effect" on ethanol metabolism [32]. In this paper, we augment the PBPK model with elements of systems biology via integrating a genome-scale model (GEM) to provide further insight into how inter-individual differences can lead to variations in the metabolism of ethanol and acetaldehyde, ultimately navigating towards precision medicine.

Precision medicine seeks to create personalized computational models of the human body to predict the impact of various therapeutic approaches [33]. Using the constraint-based reconstruction and analysis approach (COBRA), the Harvey-Harvetta GEM developed by Thiele et al. expands upon the molecular networks in previous human GEMs by integrating organ anatomy and physiology [34-35]. Within the male Harvey reconstruction, the protein reactions governed by genetics are expressed in a stoichiometric matrix (81094 reactions and 56452 metabolites), and the Flux Balance Analysis (FBA) technique is applied to solve for steady-state reaction fluxes given a specified objective function [36]. Here, we employ dynamic FBA on the Harvey GEM to perform unsteady-state characterization of ethanol metabolism, pharmacokinetics, and pharmacodynamics. By combining the PBPK model which predicts ethanol distribution throughout the body with a GEM which predicts ethanol metabolism at the organ and molecular levels, we are able to harness the benefits of both model types to create a framework that can allow for better personalized predictions of metabolism.

4.3 Methods

4.3.1 Physiologically-Based Pharmacokinetic (PBPK) Model Development

The PBPK model used to track the distribution of ethanol concentrations expands on a previously published model by having individual compartments for the stomach, small intestines and large intestines instead of a single gut compartment. This separation distinguishes between those organs' tissue and lumen for better predictions of absorption kinetics [32]. This model breaks down the human body into 14 tissue compartments (consisting of the lung, liver, stomach, small intestines, large intestines, pancreas, spleen, kidney, skin, muscle, adipose, brain, heart, and blood) and 3 lumenal compartments (consisting of the stomach, small intestines, and large intestines). A schematic of the model can be found in *Figure 4.1*.

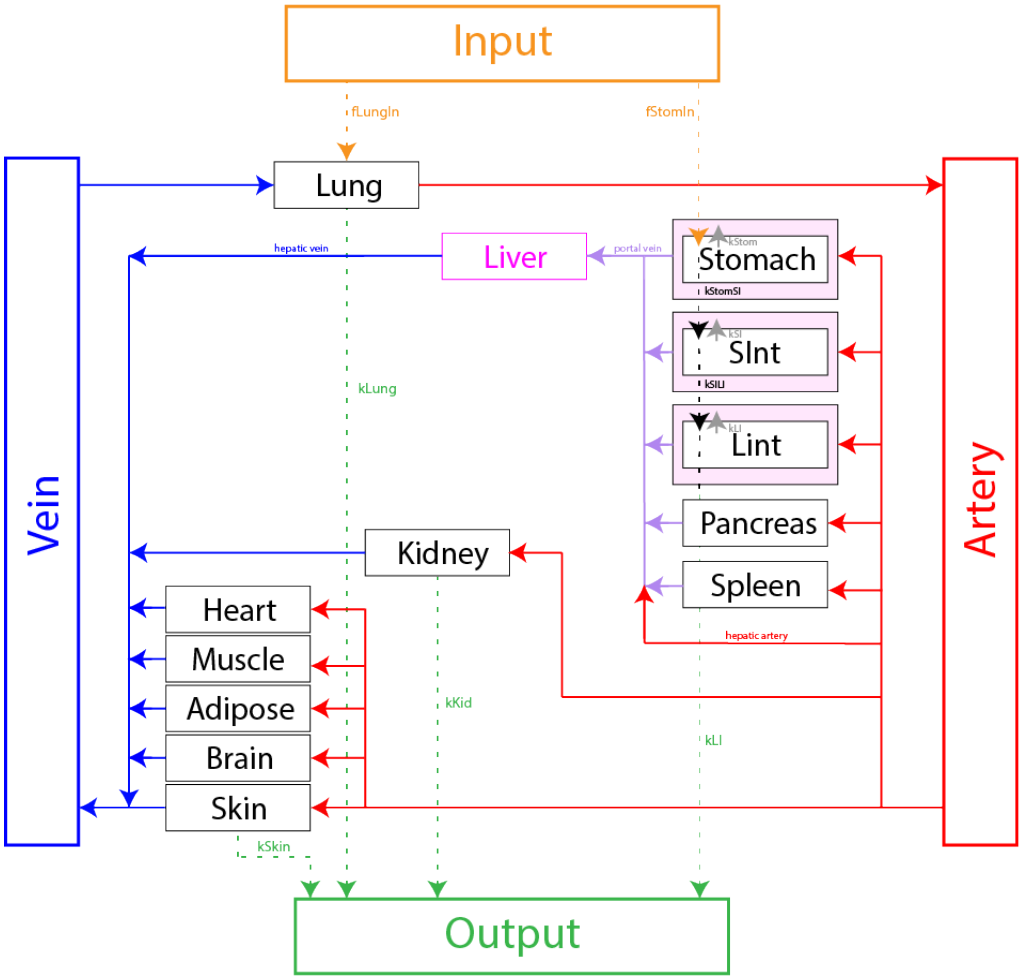

Fig. 4.1 Schematic of the PBPK model. The red, blue, and purple lines denote arterial, venous, and hepatic portal blood flows, respectively. There are two mixing points in the model at the lung and at the liver to account for their respective physiology. The model includes inputs at the lung and stomach, and outputs at the skin, kidney, lung, and large intestines.

Within the model, an individual's age, sex, height, weight, and body fat percentage are taken as model inputs to estimate the mass of various tissue compartments as well as the blood flow to each organ [37,38]. Based on the assumption that the partitioning of metabolites between tissue and plasma is in equilibrium, the drug lipophilicity and fraction unbound are used to calculate tissue-plasma partition coefficients based on tissue proportions of water, neutral lipids, and phospholipids [39,40].

The model is formulated as a system of ordinary differential equations (ODEs) which represent both the transport of metabolites across the various compartments as well as enzyme activity via Michaelis-Menten kinetics. *Equations 4.1-4.3* show the development of the ODEs from mass balance. These ODEs characterize the concentration changes in each organ and are solved simultaneously using the forward Newton-Raphson numerical integration on MATLAB© (Version 9.6.0.1174912 R2019a, CPU: 2.6 GHz 6-Core Intel Core i7, RAM: 16 GB 2667 MHz DDR4, OS: macOS Catalina 10.15.6) at each time step.

In these ODEs, organ blood flow (Q_i) and organ volume (V_i) were physiological parameters calculated by correlations with age, sex, height, weight, and body fat percentage [37]. The tissue partition coefficient (K_i) represents the pharmacokinetic properties of metabolites in the various compartments and was calculated based on the metabolite's lipophilicity, fraction unbound in the blood, and tissue composition [39]. The absorption rate constant (k_i) refers to the first-order absorption of metabolites from the organs and the transport rate constants (k_{ij}) refer to the transport of Ethanol between organs. R_i refers to any potential reactions that may occur in the tissue, characterized by either Michaelis-Menten kinetics or the genome-scale model. The generic equation for many compartments is shown in *Equation 4.3*. For the complete set of tissue-specific equations, please refer to Appendix (7.2.1).

Table 4.1 Pharmacokinetic Parameters for Ethanol and Acetaldehyde

Parameter	Ethanol	Acetaldehyde	Unit
Molecular Weight	46.07	44.05	g/mol
Lipophilicity (Log K_{ow})	-0.31	-0.34	
Fraction Unbound	0.99	0.99	

$$\mathbf{accumulation} = \mathbf{in} - \mathbf{out} + \mathbf{generation} - \mathbf{consumed} \quad (4.1)$$

$$\Delta\text{concentration} = \text{artery} - \text{vein} - \text{excretion} - \text{metabolized} \quad (4.2)$$

$$\frac{dC_i}{dt} = \frac{Q_i}{V_i}\left(C_{blood} - \frac{C_i}{K_i}\right) - k_i C_i - R_i, \text{where } R_i = \left(\frac{V_{max} C}{V_{max} + K_m}\right)_i \quad (4.3)$$

Table 4.2 Parameters used in model ODE development

Parameter	Definition	Units	Source
C_i	Concentration of metabolite in organ i	mM	Experimental
Q_i	Blood flow rate to organ i	L/min	[37]
V_i	Volume of organ i	L	[37]
K_i	Tissue:Blood partition coefficient between organ i and blood	mM/mM	[39]
k_i	Absorption rate of metabolite in organ i	1/min	Fitted
k_{ij}	Transport rate of metabolite between organ i and j	1/min	Fitted
R_i	Metabolism of metabolite in organ i	mM/min	[35]
V_{max}	V_{max} from Michaelis-Menten Kinetics	mM/min	[11]
K_m	Michaelis-Menten Constant	mM	[11]

4.3.2 Genome-Scale Model (GEM) Development

The male Harvey Model consists of 81094 reactions and 56452 metabolites [35]. In this work, we focus specifically on the exchange and metabolism of ethanol and acetaldehyde, shown in *Figures 4.2*. To generate this schematic, all ethanol and acetaldehyde species were found in the model, and related reactions were found with the function findRxnsFromMets in COBRA Toolbox [34]. The full list of reactions can be found in the Appendix (7.2.2, 7.2.3). Unique reactions were compiled and manually curated to generate the schematics.

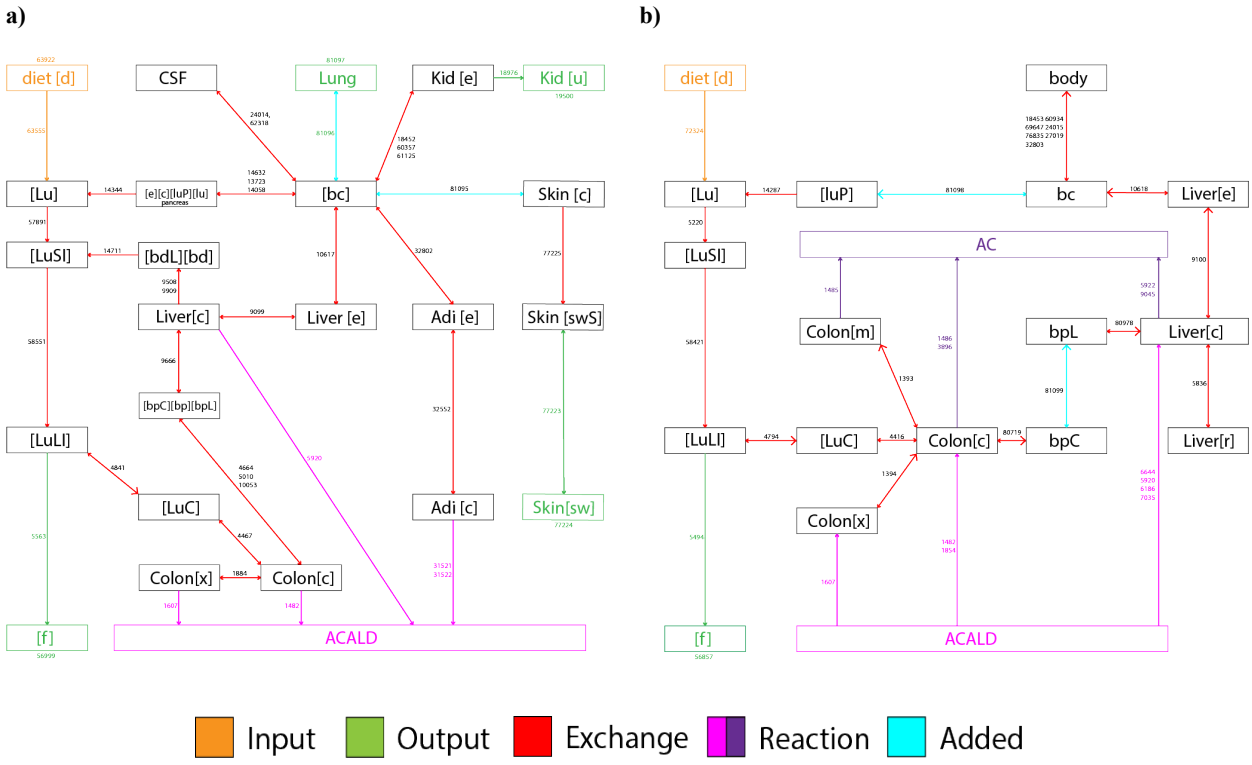

Fig. 4.2 (a) Schematic for Ethanol metabolism into Acetaldehyde (ACALD) in the Harvey model. **(b)** Schematic for Acetaldehyde (ACALD) metabolism into Acetate (AC) in the Harvey model. The orange lines denote model inputs and the green lines denote model outputs. The magenta and purple lines denote metabolism, and the blue lines are reactions that were added to Harvey to ensure consistency with the PBPK model. The numbers accompanying the arrows are the reaction numbers. For a complete list of reactions please refer to the Appendix (7.2.2, 7.2.3).

4.3.3 PBPK-GEM Integration

The PBPK model and GEM have slight differences in their inputs and outputs for metabolites, thus additional reactions were added using the Cobra function addReaction for consistency. The list of ethanol-related reactions can be found in *Table 4.3* accompanied by each reaction's amount of contribution to the overall metabolism of ethanol. All of the acetaldehyde species were eliminated by aldehyde dehydrogenases in the colon and liver (See Appendix 7.2.2, 7.2.3).

Table 4.3 Reactions involved in ethanol metabolism and elimination

	Harvey Reaction Name	PK	% of metabolism	Notes
In	'Diet_EX_etoh[d]'	Input		Diet intake
Out	'EX_etoh_[br]'	kLungout	0.05%	Lung/Breath [31, 41]
	'EX_etoh[u]'	kKid	3-10%	Urine Excretion [41]
	'EX_etoh[sw]'	kSkin	3-10%	Sweat Excretion [41]
	'Excretion_EX_etoh[fe]'	kLI	0	Feces Excretion [41]
	'Liver_ALCD2if'	rliv	90-95%	Liver ADH [27, 41-44]
	'Colon_CAT2p'	rLI	0-2%	Colon Catalase [6]
	'Colon_ALCD2if' 'Adipocytes_ALCD2if' 'Adipocytes_ALCD2yf'	N/A	0	Colon/Adipose ADH [43]

Integration of the two models employs dynamic FBA (See Equation 4.4), in which an objective function ($f^T v$) is maximized subject to a set of constraints [36]. Here, the Michaelis-Menten parameters in the PBPK model were used to set boundaries for the GEM liver alcohol dehydrogenase (ADH) and aldehyde dehydrogenase (ALDH2) reactions [45]. The objective was to maximize the amount of ethanol removed by the liver alcohol dehydrogenase ('Liver_ALCD2if'). Given that the liver accounts for 90-95% of total ethanol metabolism, the boundaries for the other reactions were calculated and constrained based on the liver metabolism rate [41-44].

To solve the model, FBA is performed with the function SolveCobraLPCPLEX, and the fluxes from the solution are used to update the PBPK model for the next time step. The FBA flux solutions are continuously used in the solver until their values deviate from the Michaelis-Menten rate past an acceptable tolerance range (typically 1-2.5%), shown by equation 4.5, after which the GEM is solved again to update the fluxes. A schematic of this process is shown in *Figure 4.3*.

$$\begin{aligned} &\mathbf{max} \quad \mathbf{f^T v} \\ &\mathbf{subject\ to\ Sv = 0} \\ &\mathbf{and\ lb_i < v_i < ub_i} \\ &\mathbf{where\ ub_i = \frac{V_{max} C_i}{K_m + C_i}} \end{aligned} \tag{4.4}$$

$$\left| \frac{r_{MM} - r_{FBA}}{r_{MM}} \right| < \text{tol} \tag{4.5}$$

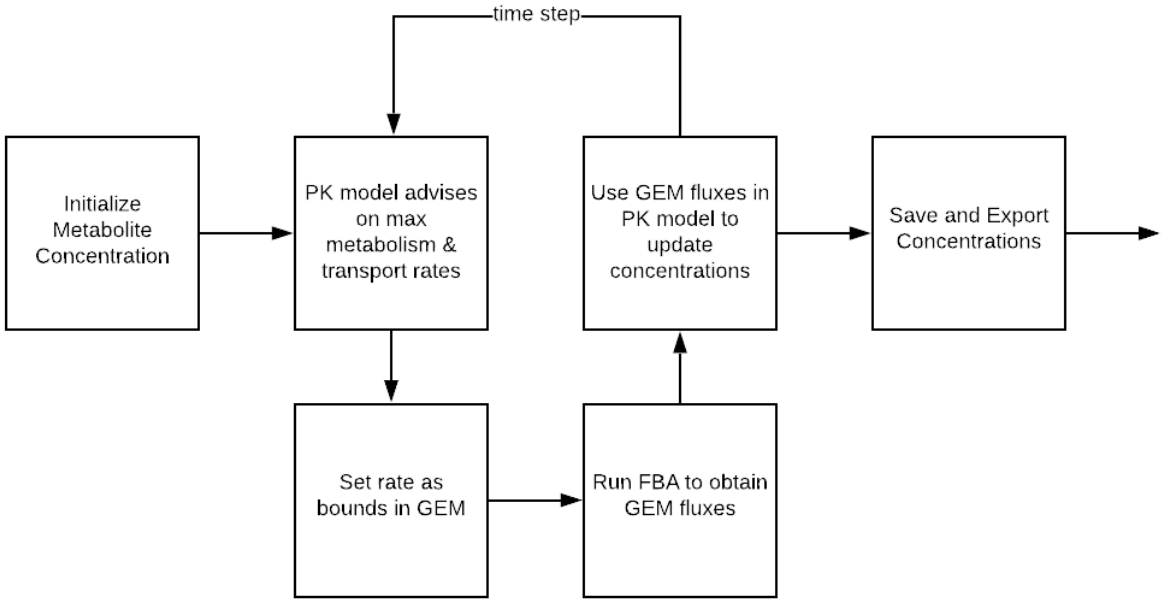

Fig. 4.3 Schematic for the dynamic Flux Balance Analysis process for integrating a GEM with a PK model.

4.4 Simulation Results & Discussion

4.4.1 Predicting the Effect of Drink Concentrations based on Fitted Model

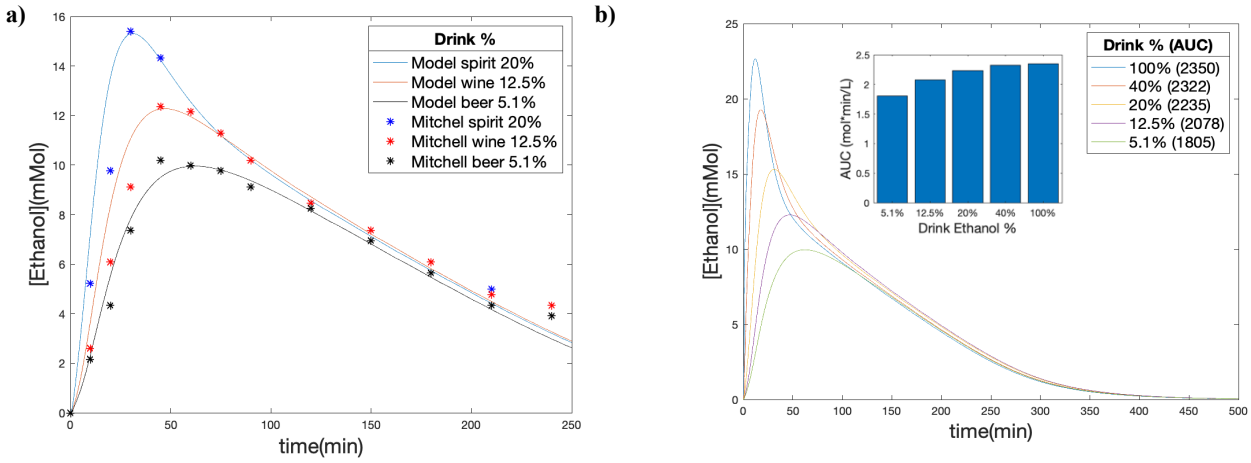

Fig. 4.4 Effect of ingested ethanol concentration on absorption kinetics. (a) Our model fitted to data from Mitchell et al. [46]. We varied absorption (k_{Stom}, k_{SI}) and transport (k_{StomSI}) parameters in the PBPK model with a V_{max} of 1.5mM/min to fit the data for beverages with concentrations of 20%, 12.5%, and 5.1% by a group of men with an average age of 37.8, mass of 82.66 kg, height of 177.1 cm and body fat of 20% controlled to 0.5g ethanol/kg. **(b)** Predictions made with the fitted model for other alcohol concentrations in a simulated male with the average characteristics of those in the data set. The inset curve shows the AUC for the different concentrations.

To first adjust the PK model to account for the added gut components (stomach, small intestines, large intestines) we fitted the model to data from Mitchell et al. to develop correlations between drink concentration and its absorption and transport through the gastrointestinal tract (*Figure 4.4a*) [46]. Ethanol is primarily absorbed by the stomach and the small intestines, so we fit k_{Stom} and k_{SI} (absorption rates for the stomach and small intestines) as well as k_{StomSI} (transport rate from the stomach to the small intestines) to achieve this fit [31,41]. These correlations can be found in Appendix 7.2.4. The Mean Absolute Error (MAE) for the fitted beer (5.1%), wine (12.5%), and spirit (20%) simulations were 0.333, 0.6066, and 0.6858, respectively. Furthermore, the model's Areas Under the Curve ($AUC_{0-\infty}$) were 1612, 1861, and 2024 mmol*min/L compared to Mitchell et al. $AUC_{0-\infty}$ of 1502, 1697, and 1871 mmol*min/L. This similarity in $AUC_{0-\infty}$ shows that the model is fairly consistent with clinical data in representing the overall systemic exposure to ethanol.

With the fitted model we made predictions for additional concentrations of ethanol. This simulation shows that as the concentration of ethanol increases, speed of absorption by the gut increases, which leads to a higher maximum concentration at a lower time. This different in absorption rate and systemic distribution is shown by the changes in the shape of the curve near the maximum concentration. After the ethanol is absorbed and distributed, the time-concentration curves behave similarly regardless of concentration because ADH is operating at V_{max}. This is demonstrated by the overlapping curves for the various drink in *Figure 4.4b*. As the concentration of ethanol falls and the ADH becomes subsaturated, the Michaelis-Menten kinetics become prominent as indicated by curvilinear elimination below concentrations of 4 mmol/L. Sustained tissue release could also be an effect here. Furthermore, drinks with higher ethanol concentrations lead to a higher exposure to ethanol as indicated by the increased AUC in the inset of *Figure 4.4b*.

4.4.2 Predicting Acetaldehyde Exposure with Fitted Model

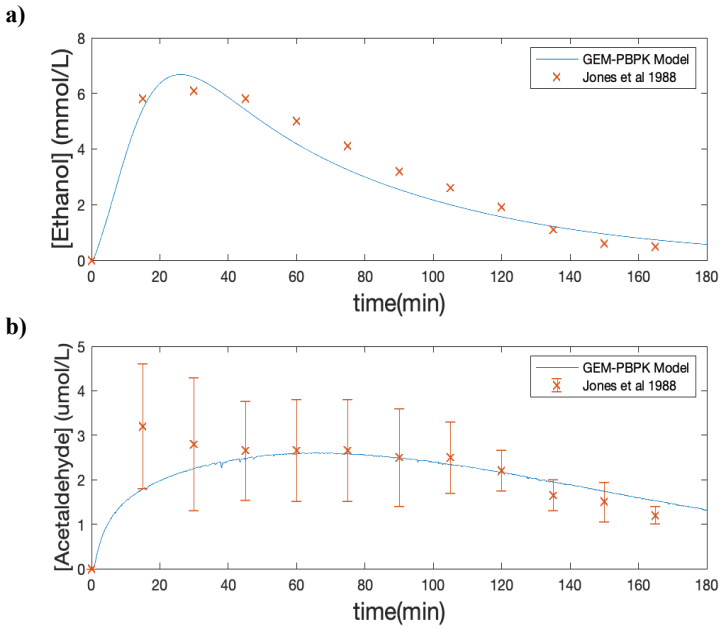

Fig. 4.5 Fitting the GEM-PBPK Model with the data from Umulis et al. [11]. (a) Our gut-absorption fitted model was fitted by changing the Michaelis-Menten kinetics and physiological parameters to match that of Umulis et al. The simulation was performed on a group of men with an average age of 25.6, mass of 74.5 kg, height of 180 cm and body fat of 20% controlled to 0.25g ethanol/kg. Simulations were performed with a tolerance of 0.1%. **(b)** Predictions made with the fitted model for acetaldehyde concentrations in a simulated male with the same average characteristics.

After fitting the model for ethanol absorption and clearance, we investigated the ability of the model to make predictions on acetaldehyde exposure as well. Umulis et al. created a PK model to predict both ethanol and acetaldehyde concentrations and compared the results to a clinical study by Jones et al. [11][47]. We used the Michaelis-Menten parameters from the Umulis et al. model to advise on the elimination kinetics of ADH and ALDH2, and the results of the simulation are shown in *Figure 4.5*.

The model produced AUCs of 526.14 mmol*min/L and 377.72 umol*min/L for ethanol and acetaldehyde, respectively, while the experimental data had AUCs of 538.5 mmol*min/L and 353.25. The similarity in AUC shows that the model can accurately capture the overall exposure to the metabolites, and the fit for the ethanol model was good with a MAE of 0.4096. Umulis et al. had difficulties characterizing the initial acetaldehyde concentrations, and given that we used the same kinetic parameters, it was expected that our models would have a similar fit. Indeed the MAE for our model was 2.1230, indicating poor fit. While the GEM-PBPK model makes similar predictions to the Umulis model, it is worth noting that there are differences, likely attributed to the model size and reactions. The Umulis model had 5 compartments and metabolism exclusively by the liver, whereas the GEM-PBPK model had 17 compartments and had 9 different reactions characterizing the metabolism of ethanol and acetaldehyde in different organs.

The smoothness of the curve generated by our model relies heavily on the simulation tolerance. In *Figure 4.5*, the tolerance was set to 0.1%, resulting in 1347 FBA iterations for the 1800 time steps. A smoother curve could be achieved with more iterations, demonstrating the trade-off between accuracy and computational intensity. For more information on the effect of tolerance on curve smoothness, please refer to Appendix 7.2.5.

4.4.3 Impact of Liver Damage on Ethanol Metabolism

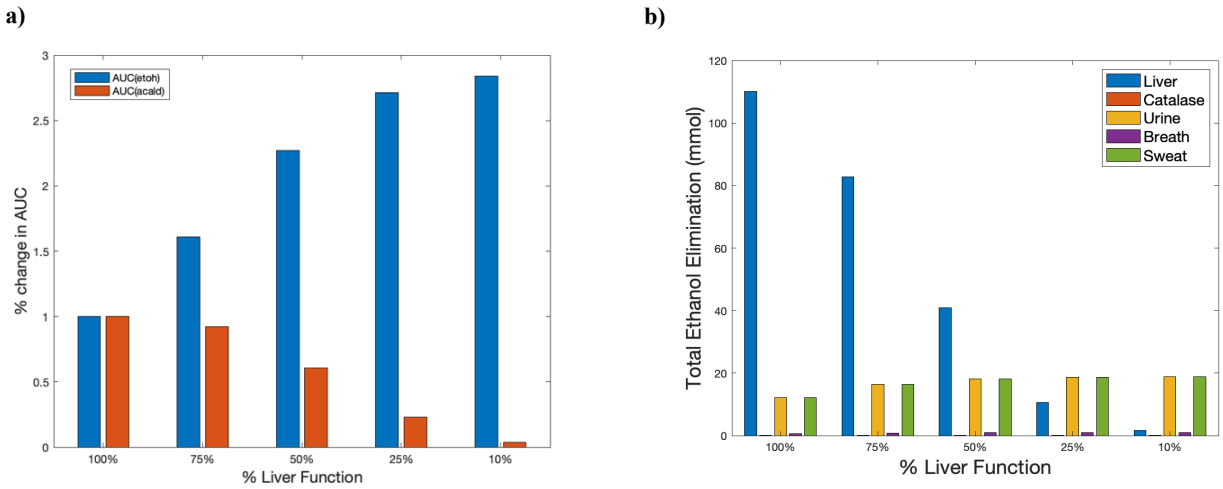

Fig. 4.6 Effect of liver impairment on ethanol metabolism. (a) Relative changes in ethanol exposure (characterized by AUC) as a result of changing liver function. The simulation was performed with the fitted model on a group of men with an average age of 25.6, mass of 74.5 kg, height of 180 cm and body fat of 20% controlled to 0.25g ethanol/kg for a total of 180 minutes. See Appendix 7.2.6 for tabulated values. **(b)** Predictions made with the fitted model for the total elimination by various processes over the 180 minutes in a simulated male with the same average characteristics.

Since the Harvey GEM can capture many pathways and find alternative ways to eliminate metabolites if specific reactions are blocked, characterized the effects of liver damage on elimination, a common symptom of alcohol abuse. Specifically, we limited the upper bounds of both the liver alcohol metabolism reaction and acetaldehyde reactions to a fraction of the V_{max} to account for various degrees of damage. The simulations showed that other processes can carry more flux to compensate for liver impairment, yet the overall metabolism rate is decreased, shown by the increase in AUC (*Figure 4.6a*). This likely occurs because at 100% liver function, the sweat and urine would eliminate at the lower bound of 3% total metabolism, but as the liver deteriorates, the sweat and urine fluxes would increase until they reach the upper bound of 10% of total metabolism (*Figure 4.6b*). Interestingly, simulations with higher degrees of liver damage have lower exposure to acetaldehyde (*Figure 4.6a*), which is consistent with clinical observations made by Wicht et al. [14]. Also, due to the lower alcohol dehydrogenase function, they have higher overall exposure to ethanol since they cannot eliminate it as effectively. For the time-concentration plots of this simulation, please refer to Appendix 7.2.6.

4.4.4 Predicting Effect of Genetic Polymorphisms on Acetaldehyde Exposure

Table 4.4 Effect of ALDH2 mutations on enzyme activity [48]

ALDH2 Isoform	Mutation	Allelic Frequency	Major Ethnicity	% of WT activity
ALDH2.1	WT			100
ALDH2.2	E504K	26.6%	East Asia	1.5
ALDH2.3	I41V	0.6%	African	60
ALDH2.4	P92T	2.5%	Latino	32.5
ALDH2.5	T244M	0.4%	South Asian	36
ALDH2.6	V304M	2.7%	Latino	12.5
ALDH2.7	R338W	1.2%	Finnish	23

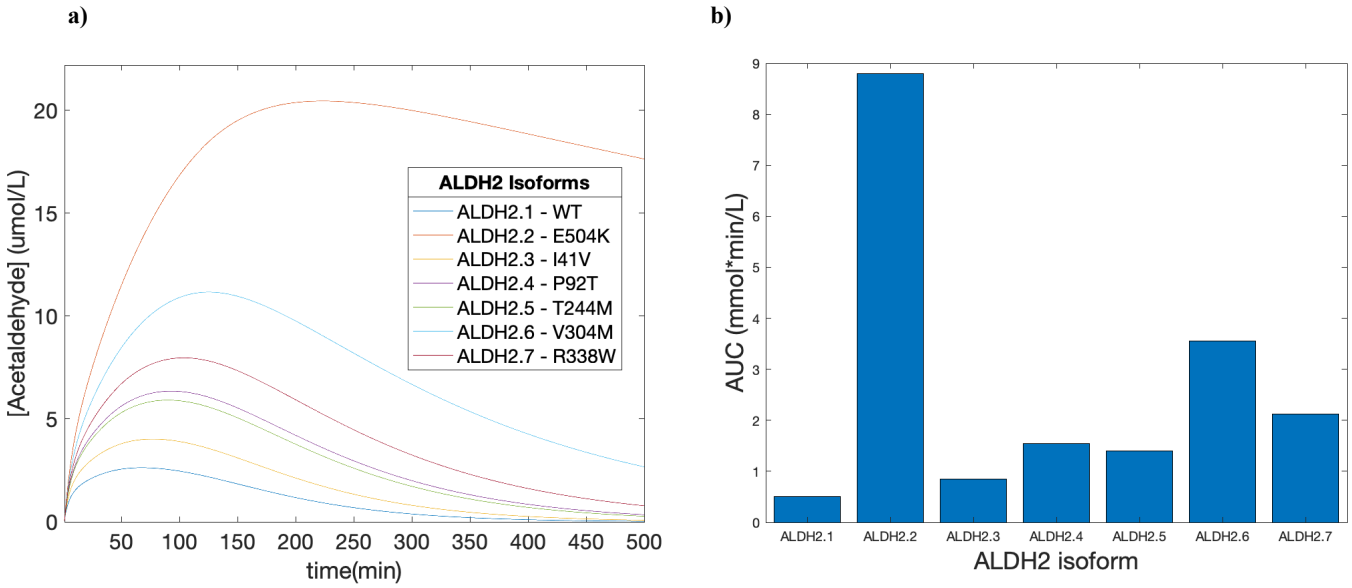

Fig. 4.7 Effect of ALDH2 mutations on acetaldehyde exposure. (a) Time-concentration plots for the effect of various ALDH2 mutations on acetaldehyde concentrations were created by changing the enzyme efficiency. The simulation was performed with the fitted model on a group of men with an average age of 25.6, mass of 74.5 kg, height of 180 cm and body fat of 20% controlled to 0.25g ethanol/kg for a total of 500 minutes. **(b)** Predictions made with the fitted model for the total systemic exposure ($AUC_{0\text{-}500}$) by various genotypes. $AUC_{0\text{-}500}$ was used instead of $AUC_{0\text{-}\infty}$ because the ALDH2.2 genotype takes over 2000 minutes to eliminate, which would lead to very large differences in AUC.

Chen et al. found significant differences in the activity of various ALDH2 isoforms compared to the wildtype [48]. Given that the rate of acetaldehyde elimination via ALDH2 is highly dependent on individual genetics, we performed simulations to characterize how different isoforms can lead to differential exposure to acetaldehyde (*Figure 4.7a*). In the ALDH2.2 isoform, which is found primarily in the East Asian population, our model predicted a 17-fold increase in exposure in the first 500 minutes when compared to the wildtype (*Figure 4.7b*). In other isoforms we saw an increase in AUC as well, but none as large as the ALDH2.2 mutation. The results of this model agree with current literature which states that individuals with the ALDH2.2 isoform have a higher exposure to acetaldehyde and additional measures must be taken to minimize potential harmful effects [10].

4.4.5 Impact of Disulfiram on Acetaldehyde Exposure

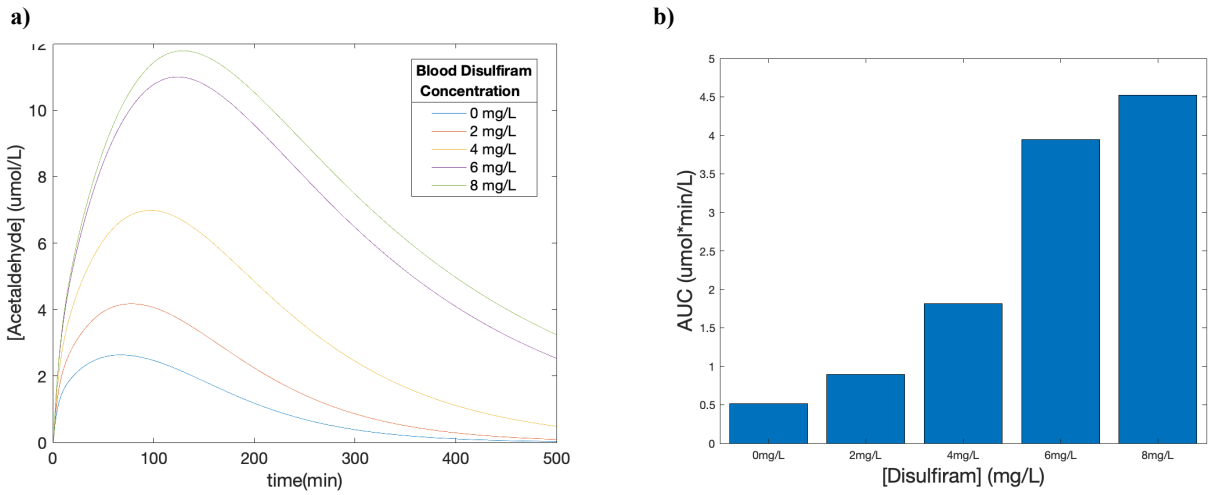

Fig. 4.8 Effect of blood disulfiram concentrations on acetaldehyde exposure. (a) Time-concentration plots of the effect of various blood disulfiram levels on acetaldehyde concentrations were created by using correlations generated from Kitson et al. [49]. The simulation was performed with the fitted model on a group of men with an average age of 25.6, mass of 74.5 kg, height of 180 cm and body fat of 20% controlled to 0.25g ethanol/kg for a total of 500 minutes. **(b)** Predictions made with the fitted model for the total systemic exposure to acetaldehyde. .

Individuals using disulfiram (Antabuse) to treat alcohol dependency can experience higher exposure to acetaldehyde, similar to individuals with the ALDH2.2 isoform. We correlated the effect of disulfiram on sheep liver ALDH based on data presented by Kitson et al. (See Appendix 7.2.7) [49]. We used a clinically relevant constant blood Disulfiram level of 2-8mg/L to characterize its effect on acetaldehyde elimination and the results of this simulation are presented in *Figure 4.8* [49]. As the blood disulfiram concentration increases, the accumulation of acetaldehyde lasts longer and ultimately leads to more exposure as shown by the increases in $AUC_{0-\infty}$ (*Figure 4.8b*).

4.4.6 Multi-dosing regimen

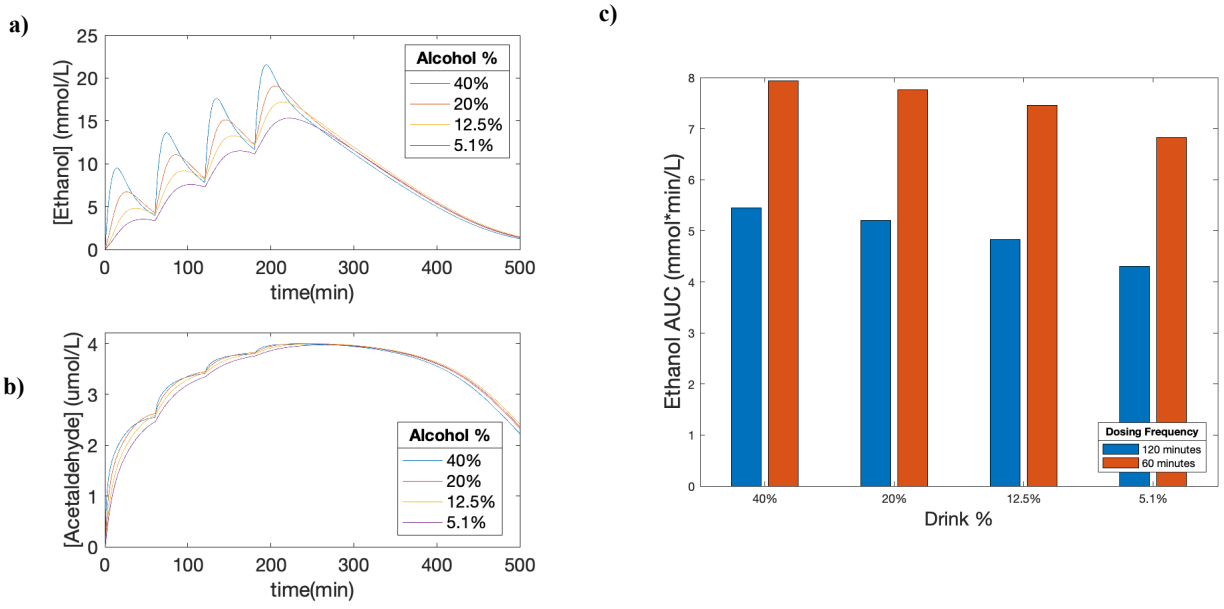

Fig. 4.9 Effect of multi-dosing on ethanol metabolism (a,b) Time-concentration plots of various alcoholic drinks on ethanol and acetaldehyde concentrations were created with a dosing frequency of 60 minutes. The simulation was performed with the fitted model on a group of men with an average age of 25.6, mass of 74.5 kg, height of 180 cm and body fat of 20% controlled to 0.25g ethanol/kg for a total of 500 minutes. **(c)** Predictions made with the fitted model for the total systemic exposure to ethanol based on drink concentration and dosing frequency.

Given that ethanol is often consumed in social settings and not in one large dose instantly, we investigated the effects of taking multiple doses of ethanol within a period. We simulated a dose every 60 minutes (*Figure 4.9a*) and 120 minutes (See Appendix 7.2.8). Once again, this revealed that exposure to ethanol increases with drink concentration (*Figure 4.9c*). Furthermore, because acetaldehyde production is based on ethanol elimination, there is no decrease in acetaldehyde concentration in the 60-minute dosing regimen until the individual stops drinking and the ethanol concentrations begin to decrease (*Figure 4.9b*). This implies that even when limiting drinks to every 60-minutes to avoid high ethanol concentrations, people could potentially be exposing themselves to higher levels of accumulated acetaldehyde than expected. Furthermore, the utility of a PBPK model allows for characterizing the overall exposures in each organ as well, potentially informing on assoated risks (See Appendix 7.2.8). Simply put, ethanol metabolism occurs at a faster rate than acetaldehyde and precaution must be taken.

4.4.7 Model Limitations

The main goal of this study was to experimentally demonstrate that this combined model can be fitted to clinical data and be used to understand the effects of ethanol and acetaldehyde as well as factors that affect the metabolism of the two molecules in the human body. Some limitations of the model include the following:

Since the Harvey model has irreversible alcohol dehydrogenase reaction, there is no reverse reaction accounted for which may have an impact in populations who are not able to metabolize acetaldehyde efficiently [11]. With a buildup of acetaldehyde, the reverse reaction may become involved to lower the exposure to the metabolite.

The fit for the disulfiram inhibition of ALDH2 were created with data from sheep liver cells, which likely behave differently than human liver cells *in vivo*. Further clinical studies and data could be used to correct this fit in the future. Furthermore, the other hepatic elimination pathways for acetaldehyde were not included in this iteration of the model.

In the modelling for genetic variations, all the simulated subjects were homozygous for the ALDH2 isoform. In reality, some individuals are likely to be heterozygous, which may affect the effect enzyme elimination rates. Furthermore, the activities of enzyme isoforms were measured *in vitro*, which may not translate well to *in vivo* reaction rates.

4.5 Conclusion

In this study we combined a PBPK model with a GEM to analyze the effects of ethanol and acetaldehyde metabolism. The uptake and absorption rates in the model were varied to fit to clinical data based on alcohol concentration, and predictions were made for the effect of drink concentration, organ damage, genetic variations, disulfiram concentration, and dosing regimen. In our simulations we found that different drink concentrations lead to different shapes in the time-concentration curves, indicating different absorption rates and changing the overall systemic exposure. Furthermore, inefficiencies or lack of function in liver metabolism is supplemented by increases in the metabolic rate of other processes, yet an overall decrease in elimination occurs. Lastly, through multi-dosing simulations, we find that even at moderate alcohol consumption rates individuals are exposing themselves to the accumulation of acetaldehyde, which could be explored in the future to gauge the correlation between acetaldehyde levels and pathogenesis.

PBPK models allow for individual tissue-compartment tracking and are the industry standard for drug modelling, and GEMs are useful when kinetic information is missing or unreliable. By combining the benefits of both models, we can gain further insight into how a genetic variation in one organ can lead to downstream effects in other tissue. GEMs are useful for predicting steady state concentrations while PBPK models are useful for predicting the dynamics given a set of parameters. In the absence of human data, the combination of models can lead to a mix of approaches to fill in the gaps necessary to fully characterize metabolism. In the future, the gut absorption added in this model can allow for the integration of microbiome data for further personalization. While this model focuses on ethanol and its metabolites, this approach can be applied to other commonly measured biomarkers, perhaps enabling a comprehensive understanding of how different aspects of human metabolism are interconnected. By expanding this framework, it is possible to envision a future where tests and drugs can be given to an individualized *in silico* metabolomic “twin” to ensure safety and efficacy prior to actual administration, ultimately moving towards precision medicine.

4.6 References

Citations formatted in accordance with PLOS Computational Biology

[1] World Health Organization. Global status report on alcohol and health. Geneva: World Health Organization; 2018. Licence: CC BY-NC-SA 3.0 IGO.

[2] Jones AW. Evidence-based survey of the elimination rates of ethanol from blood with applications in forensic casework. Forensic Sci Int. 2010;200: 1–20. doi:10.1016/j.forsciint.2010.02.021

[3] Rajendram R, Rajendram R, Preedy VR. Ethanol Metabolism and Implications for Disease. Neuropathology of Drug Addictions and Substance Misuse. Elsevier Inc.; 2016. doi:10.1016/B978-0-12-800213-1.00035-3

[4] Hernández JA, López-Sánchez RC, Rendón-Ramírez A. Lipids and Oxidative Stress Associated with Ethanol-Induced Neurological Damage. Oxid Med Cell Longev. 2016;2016. doi:10.1155/2016/1543809

[5] Heier C, Xie H, Zimmermann R. Nonoxidative ethanol metabolism in humans—from biomarkers to bioactive lipids. IUBMB Life. 2016;68: 916–923. doi:10.1002/iub.1569

[6] Cederbaum A. Alcohol Metabolism. Clin Liver Dis. 2012;16: 1–11. doi:10.1016/j.cld.2012.08.002.ALCOHOL

[7] Wright C, Moore RD. Disulfiram treatment of alcoholism. Am J Med. 1990;88: 647–655. doi:10.1016/0002-9343(90)90534-K

[8] Edenberg HJ. The genetics of alcohol metabolism: Role of alcohol dehydrogenase and aldehyde dehydrogenase variants. Alcohol Res Heal. 2007;30: 5–13.

[9] Wang JC, Kapoor M, Goate AM. The genetics of substance dependence. Annu Rev Genomics Hum Genet. 2012;13: 241–261. doi:10.1146/annurev-genom-090711-163844

[10] Gross ER, Zambelli VO, Small BA, Ferreira JCB, Chen CH, Mochly-Rosen D. A personalized medicine approach for Asian Americans with the aldehyde dehydrogenase 2∗2 variant. Annu Rev Pharmacol Toxicol. 2015;55: 107–127. doi:10.1146/annurev-pharmtox-010814-124915

[11] Umulis DM, Gürmen NM, Singh P, Fogler HS. A physiologically based model for ethanol and acetaldehyde metabolism in human beings. Alcohol. 2005;35: 3–12. doi:n

[12] Weiss R, Cogley C. Pharmacotherapy of alcohol dependence: how and when to use disulfiram and naltrexone. Curr Psychiatr. 2002;1.

[13] Lam JP, Mays DC, Lipsky JJ. Inhibition of recombinant human mitochondrial and cytosolic aldehyde dehydrogenases by two candidates for the active metabolites of disulfiram. Biochemistry. 1997;36: 13748–13754. doi:10.1021/bi970948e

[14] Wicht F, Fisch H -U, Nelles J, Raisin J, Allemann P, Preisig R. Divergence of Ethanol and Acetaldehyde Kinetics and of the Disulfiram-Alcohol Reaction between Subjects with and without Alcoholic Liver Disease. Alcohol Clin Exp Res. 1995;19: 356–361. doi:10.1111/j.1530-0277.1995.tb01515.x

[15] Helander A, Löwenmo C, Johansson M. Distribution of acetaldehyde in human blood: Effects of ethanol and treatment with disulfiram. Alcohol Alcohol. 1993;28: 461–468. doi:10.1093/oxfordjournals.alcalc.a045412

[16] Brooks PJ, Enoch MA, Goldman D, Li TK, Yokoyama A. The alcohol flushing response: An unrecognized risk factor for esophageal cancer from alcohol consumption. PLoS Med. 2009;6: 0258–0263. doi:10.1371/journal.pmed.1000050

[17] Lachenmeier DW, Kanteres F, Rehm J. Carcinogenicity of acetaldehyde in alcoholic beverages: Risk assessment outside ethanol metabolism. Addiction. 2009;104: 533–550. doi:10.1111/j.1360-0443.2009.02516.x

[18] Chen YJ, Chen C, Wu DC, Lee CH, Wu CI, Lee JM, et al. Interactive effects of lifetime alcohol consumption and alcohol and aldehyde dehydrogenase polymorphisms on esophageal cancer risks. Int J Cancer. 2006;119: 2827–2831. doi:10.1002/ijc.22199

[19] Jelski W, Szmitkowski M. Alcohol dehydrogenase (ADH) and aldehyde dehydrogenase (ALDH) in the cancer diseases. Clin Chim Acta. 2008;395: 1–5. doi:10.1016/j.cca.2008.05.001

[20] Ylikahri RH, Huttunen MO, Eriksson CJP, Nikklä EA. Metabolic Studies on the Pathogenesis of Hangover. Eur J Clin Invest. 1974;4: 93–100. doi:10.1111/j.1365-2362.1974.tb00378.x

[21] Ylikahri RH, Leino T, Huttunen MO, Pösoö AR, Eriksson CJP, Nikkilä EA. Effects of Fructose and Glucose on Ethanol-Induced Metabolic Changes and on the Intensity of Alcohol Intoxication and Hangover. Eur J Clin Invest. 1976;6: 93–102. doi:10.1111/j.1365-2362.1976.tb00498.x

[22] Eriksson CJP. Human blood acetaldehyde concentration during ethanol oxidation (update 1982). Pharmacol Biochem Behav. 1983;18: 141–150. doi:10.1016/0091-3057(83)90162-4

[23] Marek E, Kraft WK. Ethanol Pharmacokinetics in Neonates and Infants. Curr Ther Res - Clin Exp. 2014;76: 90–97. doi:10.1016/j.curtheres.2014.09.002

[24] Wilkinson PK. Pharmacokinetics of Ethanol: A Review. Alcohol Clin Exp Res. 1980;4: 6–21. doi:10.1111/j.1530-0277.1980.tb04785.x

[25] Lundquist F, Wolthers H. The Influence of Fructose on the Kinetics of Alcohol Elimination in Man. Acta Pharmacol Toxicol (Copenh). 1958;14: 290–294. doi:10.1111/j.1600-0773.1958.tb01165.x

[26] Watson PE, Watson ID, Batt RD. Prediction of blood alcohol concentrations in human subjects. Updating the Widmark equation. J Stud Alcohol. 1981;42: 547–556. doi:10.15288/jsa.1981.42.547

[27] Crabb DW, Bosron WF, Li TK. Ethanol metabolism. Pharmacol Ther. 1987;34: 59–73. doi:10.1016/0163-7258(87)90092-1

[28] Roine RP, Gentry RT, Lim RT, Baraona E, Lieber CS. Effect of Concentration of Ingested Ethanol on Blood Alcohol Levels. Alcohol Clin Exp Res. 1991;15: 734–738. doi:10.1111/j.1530-0277.1991.tb00589.x

[29] Brown AS,. JM, Fiatarone JR, Wood P, Bennett MK, Kelly PJ, Rawlins MD, et al. The effect of gastritis on human gastric alcohol dehydrogenase activity and ethanol metabolism. Aliment Pharmacol Ther. 1995;9: 57–61. doi:10.1111/j.1365-2036.1995.tb00352.x

[30] Levitt DG. PKQuest: Measurement of intestinal absorption and first pass metabolism - Application to human ethanol pharmacokinetics. BMC Clin Pharmacol. 2002;2: 1–12. doi:10.1186/1472-6904-2-4

[31] Ramchandani VA, Bosron WF, Li TK. Research advances in ethanol metabolism. Pathol Biol. 2001;49: 676–682. doi:10.1016/S0369-8114(01)00232-2

[32] Toroghi MK, Cluett WR, Mahadevan R. Multiscale Metabolic Modeling Approach for Predicting Blood Alcohol Concentration. IEEE Life Sci Lett. 2017;2: 59–62. doi:10.1109/lls.2016.2644647
[33] Kell DB. The virtual human: Towards a global systems biology of multiscale, distributed biochemical network models. IUBMB Life. 2007;59: 689–695. doi:10.1080/15216540701694252
[34] Thiele I, Palsson B. A protocol for generating a high-quality genome-scale metabolic reconstruction. Nat Protoc. 2010;5: 93–121. doi:10.1038/nprot.2009.203
[35] Thiele I, Sahoo S, Heinken A, Hertel J, Heirendt L, Aurich MK, et al. Personalized whole-body models integrate metabolism, physiology, and the gut microbiome. Mol Syst Biol. 2020;16: 1–24. doi:10.15252/msb.20198982
[36] Orth JD, Thiele I, Palsson BO. What is flux balance analysis? Nat Biotechnol. 2010;28: 245–248. doi:10.1038/nbt.1614
[37] Stader F, Penny MA, Siccardi M, Marzolini C. A Comprehensive Framework for Physiologically-Based Pharmacokinetic Modeling in Matlab. CPT Pharmacometrics Syst Pharmacol. 2019. doi:10.1002/psp4.12399
[38] Brown RP, Delp MD, Lindstedt SL, Rhomberg LR, Beliles RP. PHYSIOLOGICALLY BASED PHARMACOKINETIC MODELS Protection Agency ; V. Toxicol Ind Health. 1997;13: 407–484.
[39] Poulin P, Theil FP. A priori prediction of tissue: Plasma partition coefficients of drugs to facilitate the use of physiologically-based pharmacokinetic models in drug discovery. J Pharm Sci. 2000;89: 16–35. doi:10.1002/(SICI)1520-6017(200001)89:1<16::AID-JPS3>3.0.CO;2-E
[40] Peters SA. Physiologically-Based Pharmacokinetic (PBPK) Modeling and Simulations: Principles, Methods, and Applications in the Pharmaceutical Industry. Physiologically-Based Pharmacokinetic (PBPK) Modeling and Simulations: Principles, Methods, and Applications in the Pharmaceutical Industry. 2012. doi:10.1002/9781118140291
[41] Norberg A, Jones AW, Hahn RG, Gabrielsson JL. Role of Variability in Explaining Ethanol Pharmacokinetics. Clin Pharmacokinet. 2003;42: 1–31. doi:10.2165/00003088-200342010-00001
[42] Jones AW, Neri A. Age-Related Differences in Blood Ethanol Parameters and Subjective Feelings of Intoxication in Healthy Men. Alcohol Alcohol. 1985;20: 45–52. doi:10.1093/oxfordjournals.alcalc.a044503
[44] Matsumoto H, Fukui Y. Pharmacokinetics of ethanol: A review of the methodology. Addict Biol. 2002;7: 5–14. doi:10.1080/135562101200100553
[45] Mahadevan R, Edwards JS, Doyle FJ. Dynamic flux balance analysis of diauxic growth. Biophys J. 2002;83: 1331–1340. Available: https://pdfs.semanticscholar.org/8d56/a26c56704266b5d7c426ecdfc286962f9112.pdf
[46] Mitchell MC, Teigen EL, Ramchandani VA. Absorption and peak blood alcohol concentration after drinking beer, wine, or spirits. Alcohol Clin Exp Res. 2014;38: 1200–1204. doi:10.1111/acer.12355
[47] Jones A, Neiman J, Hillbom M. Concentration-time profiles of ethanol and acetaldehyde in human volunteers treated with the alcohol-sensitizing drug, calcium carbimide. Br J Clin Pharmacol. 1988;25: 213–221. doi:10.1111/j.1365-2125.1988.tb03293.x

[48] Chen CH, Ferreira JCB, Joshi AU, Stevens MC, Li SJ, Hsu JHM, et al. Novel and prevalent non-East Asian ALDH2 variants; Implications for global susceptibility to aldehydes' toxicity. EBioMedicine. 2020;55: 1–11. doi:10.1016/j.ebiom.2020.102753

[49] Kitson TM. Studies on the interaction between disulfiram and sheep liver cytoplasmic aldehyde dehydrogenase. Biochem J. 1978;175: 83–90. doi:10.1042/bj1750083

[50] Malcolm MT. Disulfiram blood levels. Br Med J. 1977; 6084: 457. doi:10.1136/bmj.2.6084.457-d

5 Conclusions

5.1 THC Model

In this work, I created a PBPK model for THC metabolism and investigated the implications of various genotypes on overall exposure. Research into cannabis is flourishing and as data continues to become available, the model can be updated to better advise on a standard dosing unit for THC. This model establishes a framework for future studies to examine the effects of tolerance, inhalation technique/method, subjective effects, and the opportunity to incorporate receptor kinetics. The primary metabolite of THC, 11-OH-THC, is also psychoactive, and future work should incorporate this compound as well. The next steps for this project can involve using individual time-concentration curves to better adapt the model to various genetic polymorphisms and ultimately shape the future of cannabis health policy.

5.2 Ethanol model

By combining the benefits of both GEM and PBPK models, I developed a framework for better predictions of drug metabolism through the ability to limit (or even knock out) specific genes and proteins. With the investigation into how various amounts of liver damage leads to changes in the metabolic rate of other processes, we can gain a more comprehensive understanding of how ethanol is eliminated. Furthermore, with the work on how genotypes and ALDH2 inhibiting drugs increase the exposure to acetaldehyde, future studies can build personalized models to limit the toxicity associated with ethanol usage. While this work explored the space of ethanol and acetaldehyde metabolism, a potential direction that could change the future of precision medicine can involve building a GEM-PBPK model surrounding all of the common metabolites measured in a clinical blood-test. The GEM steady state fluxes can gap fill the PBPK model where there is not enough kinetic data available. This comprehensive model is a starting step towards dynamic mapping of the human metabolic atlas, and eventually allow for an *in-silico* virtual twins to be created for drug testing prior to actual administration. With an expansion on the methodology presented in this work, the field of pharmacokinetic modelling can take a large step towards actualizing precision medicine.

6 Significance, Limitations and Future Work

6.1 Significance

In the cannabis space, the metabolism of THC is not well understood, and predictive models are often simple and do not represent human physiology. Through the work here, we fitted our PBPK model to clinical data, which allowed for predictions based on a variety of interindividual differences. Furthermore, to characterize the effects of THC more objectively, we correlated the blood concentrations of THC to driving performance through SDLP.

In ethanol modelling, while the metabolism through alcohol dehydrogenase is well characterized, there is a gap in a holistic view of the different available pathways. By integrating a GEM to advise on other routes of elimination, the model expands beyond ethanol metabolism but also incorporates reactions that eliminate its downstream metabolite, acetaldehyde, as well. The significance of this work lies in the potential utility of an integrated GEM-PBPK model. Using this framework, we were able to predict for the effects of genetic differences in populations as well as the exposures of various organs to ethanol and acetaldehyde.

GEMs have been compiled for the last few decades, and while they are comprehensive there is the possibility of human errors and inconsistencies in metabolic reactions. Thus, by curating the ethanol metabolism portion of the integrated model, a small fraction of the entire Harvey model was revised. By finding the differences between GEMs and published literature, we are able to identify the potential biochemical gaps in the field, and can navigate future research towards a more comprehensive understanding of the body.

With information about how genetics play a role in the GEM, future iterations of the model can relate an individual's sequencing to specific gene functions, ultimately advising on the efficiency of various processes. Specifically, the GEM accounts for the steady-state metabolism of processes, but when combined with a PK model through dynamic FBA, the transient metabolism of substances after a perturbation can be calculated as well.

Overall, a very interesting application of this framework exists in anesthesiology, where multiple drugs are given to a vast variety of people, allowing for continuous refinement of the model with clinical data for future optimizations. However, to reach this epitome of precision medicine, there are a few limitations of the model that must be addressed.

6.2 Limitations

One of the primary limitations of the model falls within the field of PBPK modelling. On one hand, a model that is too simple cannot provide accurate predictions, but alternatively a model that is too complex requires either large amounts of clinical data (much of which is unavailable or even unattainable), or may require overfitting.

In terms of complexity, the current state of PBPK models generalize most tissues to a single compartment, and may not fully capture the physiology behind organs. For example, in the PBPK models here, the hepatic portal vein and the hepatic artery mix prior to entering the single-compartment liver, whereas in physiology they supply different lobes of the liver. While this can be accounted for in the model, it leaves many questions to be asked regarding transport rates between the lobes, the degree of mixing, and many inquiries that are difficult to study in actual humans. These parameters would need to be either supported by allometric data from animals, or fitted to existing clinical data. This distribution of drugs may involve the influence of fed-state, tolerance, and many other factors.

Furthermore, the metabolism of drugs can involve the induction and inhibition of enzymes, especially within the cytochrome P450 family. Given that the GEM-PBPK model accounts for some levels of gene expression, future experimentation can investigate the transcriptomics behind the enzymes to characterize the effect of various activating and deactivating factors.

With respect to the enzyme-substrate kinetics, some enzymes are promiscuous in their function, allowing for the metabolism of other substances as well. One example is that the CYP2C9 enzyme is responsible for THC elimination, but also warfarin and phenytoin. In circumstances where competitive inhibition may occur, it would be beneficial add in those kinetics into the

Michaelis-Menten equations as well. For one substrate, this is simple, but when extending this approach to a collection of metabolites and possible drug combinations, it becomes a fairly arduous task.

Since the metabolic pathways are so robust, PBPK models can only focus on a collection of reactions at a time. In the ethanol mode, while there are other metabolic pathways for acetaldehyde, only the aldehyde dehydrogenase reaction was modeled due to a lack of both kinetic data for the PK aspect and a lack of genes representing the other pathways in the GEM. This limitation shows that much more work must be done to comprehensively understand metabolism.

Lastly, a limitation of this work involves the usage of AUC as a measurement of the goodness of fit. Typically, a chi-squared analysis would be appropriate for gauging whether or not the predictions are representative of the population, yet with few clinical data points it was not possible to obtain statistically significant results. With data from individuals instead of populations, this analysis would be much more productive and the model would even better.

6.3 Future Work

There are many possible areas of improvement for PBPK modelling, and I believe that there is great potential for the GEM-PBPK framework to influence the field of precision medicine. One important aspect that should be addressed in future models would be to resolve the issues with the liver physiology. While it may not make a drastic difference in the overall metabolic rate, it is important to apply scientific rigor and ensure physiological consistency.

After correcting for the liver, there's two possible paths to pursue. First, the GEM-PBPK model can delve deeper into its integration by incorporating the metabolism of not only ethanol, but also more common metabolites in the body. There are over 50,000 metabolites present in Harvey, but a good starting point could involve investigating the metabolism of the species currently characterized by yearly physical exams' blood work. With this comprehensive model

and large amounts of data related to the patient's genome sequencing, we can start gauging how a person's physiological, genomic, and epidemiological factors play into the development of diseases. Consequently, the effect of various drugs can be investigated *in silico* to investigate the effects of potential treatments as well.

A different path could involve deeply understand the metabolism of one particular substance. In the GEM-PBPK model here, there were nine reactions characterizing the metabolism of ethanol and acetaldehyde, while many other processes exist. By doing a thorough literature review on the complete elimination of ethanol and its metabolites, an even more comprehensive model of ethanol metabolism can be created. If it were possible to acquire information on the *in vivo* enzyme kinetics associated with each process and enzyme isoform, the model would become very predictive after rigorous testing and could potentially even lead to advancements in forensics practices.

Overall, the GEM-PBPK model provides an interesting combination between the pharmacological field with systems biology. GEMs can advise on how different metabolic processes interact with each other at steady state, while PBPK models enable insight into the dynamics over a period of time. By complementing each other and compensating for each model's weaknesses, the integrated GEM-PBPK model can potentially play a significant role in furthering the field of precision medicine.

7 Appendices

7.1 THC Appendices

7.1.1 THC PBPK Model Development

Tissue-specific model equations:

$$\frac{dC_i}{dt} = \frac{Q_i}{V_i}\left(C_{blood} - \frac{C_i}{K_i}\right) \quad \text{SI.1}$$

The equation for the arterial blood concentration is:

$$\frac{dC_{Blood}}{dt} = \frac{Q_{Lung}}{V_{Lung}}\left(\frac{C_{Lung}}{K_{Lung}} - C_{Blood}\right) \quad \text{SI.2}$$

The equations for the lungs and kidneys are shown below. The k_i represents the clearance rate by organ i to the outside environment.

$$\frac{dC_{Lung}}{dt} = \frac{Q_{Lung}}{V_{Lung}}\left(C_{Vein} - \frac{C_{Lung}}{K_{Lung}}\right) - k_{Lung} * C_{Lung} \quad \text{SI.3}$$

$$\frac{dC_{Kid}}{dt} = \frac{Q_{Kid}}{V_{Kid}}\left(C_{Blood} - \frac{C_{Kid}}{K_{Kid}}\right) - k_{Kid} * C_{Kid} \quad \text{SI.4}$$

The equations for the stomach, small and large intestines are shown below. The k_i represents the absorbance from the lumenal component of organ i into the tissue.

$$\frac{dC_{Stom}}{dt} = \frac{Q_{Stom}}{V_{Stom}}\left(C_{Blood} - \frac{C_{Stom}}{K_{Stom}}\right) + k_{Stom} * C_{L,Stom} - R_{Stom} \quad \text{SI.5}$$

$$\mathbf{\frac{dC_{SI}}{dt} = \frac{Q_{SI}}{V_{SI}}\left(C_{Blood} - \frac{C_{SI}}{K_{SI}}\right) + k_{SI} * C_{L,SI}} \quad \text{SI.6}$$

$$\frac{dC_{LI}}{dt} = \frac{Q_{LI}}{V_{LI}}\left(C_{Blood} - \frac{C_{LI}}{K_{LI}}\right) + k_{LI} * C_{L,LI} \quad \text{SI.7}$$

The equations for $Q_{Liv,in}$ and $C_{Liv,in}$ are shown below. The organs used for the calculations include the stomach, small and large intestines, pancreas, and spleen. Q_{Liv} represents the blood flow from the hepatic artery, $Q_{Liv,in}$ represents the total blood flow into the liver after the mixing of the hepatic artery with the hepatic portal vein, and $C_{Liv,in}$ represents the concentration of THC after the hepatic artery mixes with the hepatic portal vein.

$$Q_{Liv,in} = Q_{Stom} + Q_{SI} + Q_{LI} + Q_{Pancreas} + Q_{Spleen} + Q_{Liv} \quad \text{SI.8}$$

$$C_{Liv,in} = \frac{\sum_{i=1}^{5} \frac{Q_i * C_i}{K_i} + Q_{Liv} * C_{Blood}}{Q_{Liv,in}} \quad \text{SI.9}$$

The equation for C_{Vein} is shown below. C_{Vein} represents the concentration of the venous blood returning to the lungs after mixing in the heart. The organs involved include adipose, brain, heart, kidney, liver (hepatic vein), muscle, and skin:

$$C_{Vein} = \frac{\sum_{i=1}^{7} \frac{Q_i * C_i}{K_i}}{Q_{Lung}} \quad \text{SI.10}$$

The equation for the liver is:

$$\frac{dC_{Liv}}{dt} = \frac{Q_{Liv,in}}{V_{Liv}} \left(C_{Liv,in} - \frac{C_{Liv}}{K_{Liv}} \right) - R_{Liv} \quad \text{SI.11}$$

The equations for the lumenal compartments of the stomach, small intestines, and large intestines are listed below. The k_i represents the absorbance from the lumen into the tissue, and the k_j represents the transport of metabolites from the lumen of compartment i to the lumen of compartment j. In the lumenal compartments, the concentration changes are affected by the absorption of THC through the GI tract, allowing for the model to be used in oral cannabis dosing in the future.

$$\frac{dC_{L,stom}}{dt} = -(k_{stom} + k_{stomSI}) * C_{L,stom} \quad \text{SI.12}$$

$$\frac{dC_{L,SI}}{dt} = k_{stomSI} * C_{L,stom} - (k_{SI} + k_{SILI}) * C_{L,SI} \quad \text{SI.13}$$

$$\frac{dC_{L,LI}}{dt} = k_{SILI} * C_{L,SI} - (k_{LI} + k_{poop}) * C_{L,LI} \quad \text{SI.14}$$

The Cardiac Output is determined using the following equation where CO represents the cardiac output, BSA represents the body surface area and age is the age of the patient tested.

$$\mathbf{CO = (159 * BSA - 1.56 * age + 114)} \quad \text{SI.15}$$

7.2 Ethanol Model Appendices

7.2.1 Ethanol PBPK Model Development

Tissue-specific model equations:

$$\frac{dC_i}{dt} = \frac{Q_i}{V_i}\left(C_{blood} - \frac{C_i}{K_i}\right) \quad \text{SI.16}$$

The equation for the arterial blood concentration is:

$$\frac{dC_{Blood}}{dt} = \frac{Q_{Lung}}{V_{Lung}}\left(\frac{C_{Lung}}{K_{Lung}} - C_{Blood}\right) \quad \text{SI.17}$$

The equations for the lungs, kidneys, and skin are shown below. The R_i represents the clearance rate by organ i to the outside environment.

$$\frac{dC_{Lung}}{dt} = \frac{Q_{Lung}}{V_{Lung}}\left(C_{Vein} - \frac{C_{Lung}}{K_{Lung}}\right) - R_{lung} \quad \text{SI.18}$$

$$\frac{dC_{Kid}}{dt} = \frac{Q_{Kid}}{V_{Kid}}\left(C_{Blood} - \frac{C_{Kid}}{K_{Kid}}\right) - R_{Kid} \quad \text{SI.19}$$

$$\frac{dC_{Skin}}{dt} = \frac{Q_{Skin}}{V_{Skin}}\left(C_{Blood} - \frac{C_{Skin}}{K_{Skin}}\right) - R_{Skin} \quad \text{SI.20}$$

The equations for the stomach, small and large intestines are shown below. The k_i represents the absorbance from the luminal component of organ i into the tissue. The Ri represents the clearance rate by organ i to the outside environment

$$\frac{dC_{Stom}}{dt} = \frac{Q_{Stom}}{V_{Stom}}\left(C_{Blood} - \frac{C_{Stom}}{K_{Stom}}\right) + k_{Stom} * C_{L,Stom} - R_{Stom} \quad \text{SI.21}$$

$$\mathbf{\frac{dC_{SI}}{dt} = \frac{Q_{SI}}{V_{SI}}\left(C_{Blood} - \frac{C_{SI}}{K_{SI}}\right) + k_{SI} * C_{L,SI}} \quad \text{SI.22}$$

$$\frac{dC_{LI}}{dt} = \frac{Q_{LI}}{V_{LI}}\left(C_{Blood} - \frac{C_{LI}}{K_{LI}}\right) + k_{LI} * C_{L,LI} - R_{Catalase} \quad \text{SI.23}$$

The equations for $Q_{Liv,in}$ and $C_{Liv,in}$ are shown below. The organs used for the calculations include the stomach, small and large intestines, pancreas, and spleen. Q_{Liv} represents the blood flow from the hepatic artery, $Q_{Liv,in}$ represents the total blood flow into the liver after the mixing of the hepatic artery with the hepatic portal vein, and $C_{Liv,in}$ represents the concentration of THC after the hepatic artery mixes with the hepatic portal vein.

$$Q_{Liv,in} = Q_{Stom} + Q_{SI} + Q_{LI} + Q_{Pancreas} + Q_{Spleen} + Q_{Liv} \quad \text{SI.24}$$

$$C_{Liv,in} = \frac{\sum_{i=1}^{5} \frac{Q_i * C_i}{K_i} + Q_{Liv} * C_{Blood}}{Q_{Liv,in}} \quad \text{SI.25}$$

The equation for C_{Vein} is shown below. C_{Vein} represents the concentration of the venous blood returning to the lungs after mixing in the heart. The organs involved include adipose, brain, heart, kidney, liver (hepatic vein), muscle, and skin:

$$C_{Vein} = \frac{\sum_{i=1}^{7} \frac{Q_i * C_i}{K_i}}{Q_{Lung}} \quad \text{SI.26}$$

The equation for the liver is:

$$\frac{dC_{Liv}}{dt} = \frac{Q_{Liv,in}}{V_{Liv}}\left(C_{Liv,in} - \frac{C_{Liv}}{K_{Liv}}\right) - R_{Liv} \quad \text{SI.27}$$

The equations for the luminal compartments of the stomach, small intestines, and large intestines are listed below. The k_i represents the absorbance from the lumen into the tissue, and the k_j represents the transport of metabolites from the lumen of compartment I to the lumen of compartment j. In the luminal compartments, the concentration changes are affected by the absorption of THC through the GI tract, allowing for the model to be used in oral cannabis dosing in the future.

$$\frac{dC_{L,SI}}{dt} = k_{stomSI} * C_{L,stom} - (k_{SI} + k_{SILI}) * C_{L,SI} \quad \text{SI.28}$$

$$\frac{dC_{L,LI}}{dt} = k_{SILI} * C_{L,SI} - (k_{LI} + k_{poop}) * C_{L,LI} \quad \text{SI.29}$$

The Cardiac Output is determined using the following equation where CO represents the cardiac output, BSA represents the body surface area and age is the age of the patient tested.

$$\mathbf{CO = (159 * BSA - 1.56 * age + 114)} \quad \text{SI.30}$$

7.2.2 Ethanol-Related Reactions

Table SI.1 Ethanol-Related Reactions

Reaction #	Reaction Name	Reaction #	Reaction Name
1482	Alcohol Dehydrogenase, Forward Rxn (Ethanol -> Acetaldehyde) (Colon)'	18976	Exchange of Ethanol (from[e] toblood)'
1607	Catalase A, Peroxisomal (Ethanol) (Colon)'	19500	EX_etoh[u]'
1884	Transport of Ethanol, Reversible, Peroxisomal (Colon)'	24014	Ethanol MonooxygenaseTransport of Ethanol, Reversible, PeroxisomalEthanol Reversible Transport (BBB)'
3664	Biomass maintenance reaction without replication precursorsBiomass maintenance reaction without replication, transcription, and translation precursors (Colon)'	30871	Biomass maintenance reaction without replication precursorsBiomass maintenance reaction without replication, transcription, and translation precursors (Skin)'
4467	Transport of Ethanol, Reversible, PeroxisomalEthanol Reversible Transport (Colon)'	31521	Alcohol Dehydrogenase, Forward Rxn (Ethanol -> Acetaldehyde) (Adipocytes)'
4664	Transport of Ethanol, Reversible, PeroxisomalEthanol Reversible Transport (Colon)'	31522	Alcohol Dehydrogenase (Ethanol, NADP), Forward Reaction (Adipocytes)'
4841	Exchange of Ethanol (Colon)'	32552	Transport of Ethanol, Reversible, PeroxisomalEthanol Reversible Transport (Adipocytes)'
5010	Exchange of Ethanol (Colon)'	32802	Exchange of Ethanol (from[e] toblood)'
5563	Exchange of Ethanol (LI)'	56999	Exchange of Ethanol (Excretion)'
5920	Alcohol Dehydrogenase, Forward Rxn (Ethanol -> Acetaldehyde) (Liver)'	57891	Exchange of Ethanol (SI)'
9099	Transport of Ethanol, Reversible, PeroxisomalEthanol Reversible Transport (Liver)'	58551	Exchange of Ethanol (SI)'
9508	Transport of Ethanol, Reversible, PeroxisomalEthanol Reversible Transport (Liver)'	60357	Kidney_etoh(e)_[bcK]'
9666	Transport of Ethanol, Reversible, PeroxisomalEthanol Reversible Transport (Liver)'	61125	Exchange of Ethanol (Kidney)'
9909	Exchange of Ethanol (Liver)'	62318	Ethanol MonooxygenaseTransport of Ethanol, Reversible, PeroxisomalEthanol Reversible Transport (BBB)'
10053	Exchange of Ethanol (Liver)'	63555	Exchange of Ethanol (GI)'
10617	Exchange of Ethanol (from[e] toblood)'	63922	Exchange of Ethanol (Diet)'
13521	Biomass maintenance reaction without replication precursorsBiomass maintenance reaction without replication, transcription, and translation precursors (Pancreas)'	77223	Skin_EX_etoh(swS)_[sw]'
13723	Transport of Ethanol, Reversible, PeroxisomalEthanol Reversible Transport (Pancreas)'	77224	EX_etoh[sw]'
14058	Transport of Ethanol, Reversible, PeroxisomalEthanol Reversible Transport (Pancreas)'	77225	Skin_etoh_DIFF(c)_[swS]'
14344	Exchange of Ethanol (Pancreas)'	77381	Biomass maintenance reaction without replication precursorsBiomass maintenance reaction without replication, transcription, and translation precursors (Liver)'
14632	Exchange of Ethanol (frombloodto[e]'	77386	Biomass maintenance reaction without replication precursorsBiomass maintenance reaction without replication, transcription, and translation precursors (Adipocytes)'
14711	Exchange of Ethanol (BileDuct)'	81095	'Skin_EX_etoh(c)_[bc]'
17276	Biomass maintenance reaction without replication precursorsBiomass maintenance reaction without replication, transcription, and translation precursors (Kidney)'	81096	'Lung_EX_etoh(br)_[bc]'
18452	Kidney_EX_etoh(e)_[bc]'	81097	'EX_etoh[br]'

7.2.3 Acetaldehyde-Related Reactions

Table SI.2 Acetaldehyde-Related Reactions

Reaction #	Reaction Name	Reaction #	Reaction Name
1393	Acetaldehyde Mitochondrial Diffusion'	14287	Exchange of Acetaldehyde (Pancreas)'
1394	Acetaldehyde Peroxisomal Diffusion'	18453	Exchange of Acetaldehyde (frombloodto[e]'
1482	"Alcohol Dehydrogenase, Forward Rxn (Ethanol -> Acetaldehyde)"'	24015	Acetaldehyde Mitochondrial DiffusionAcetaldehyde Reversible Transport, Endoplasmatic ReticulumAcetaldehyde Peroxisomal DiffusionAcetaldehyde Reversible Transport (BBB)'
1485	"Aldehyde Dehydrogenase (Acetylaldehyde, NAD), Mitochondrial"'	27019	Exchange of Acetaldehyde (from[e] toblood)'
1486	"Aldehyde Dehydrogenase (Acetaldehyde, NADP)"'	32803	Exchange of Acetaldehyde (from[e] toblood)'
1607	"Catalase A, Peroxisomal (Ethanol)"'	34199	Exchange of Acetaldehyde (from[e] toblood)'
1854	Deoxyribose-Phosphate Aldolase'	39992	Exchange of Acetaldehyde (from[e] toblood)'
3896	"Aldehyde Dehydrogenase (Acetaldehyde, NAD)"'	43159	Exchange of Acetaldehyde (from[e] toblood)'
4416	Acetaldehyde Mitochondrial DiffusionAcetaldehyde Reversible Transport, Endoplasmatic ReticulumAcetaldehyde Peroxisomal DiffusionAcetaldehyde Reversible Transport (Colon)'	48388	Exchange of Acetaldehyde (from[e] toblood)'
4794	Exchange of Acetaldehyde (Colon)'	50162	Exchange of Acetaldehyde (from[e] toblood)'
5220	Exchange of Acetaldehyde (SI)'	52468	Exchange of Acetaldehyde (from[e] toblood)'
5494	Exchange of Acetaldehyde (LI)'	53545	Exchange of Acetaldehyde (from[e] toblood)'
5836	"Acetaldehyde Reversible Transport, Endoplasmatic Reticulum"'	54747	Exchange of Acetaldehyde (from[e] toblood)'
5920	"Alcohol Dehydrogenase, Forward Rxn (Ethanol -> Acetaldehyde)"'	55819	Exchange of Acetaldehyde (from[e] toblood)'
5922	"Aldehyde Dehydrogenase (Acetaldehyde, NADP)"'	56659	Exchange of Acetaldehyde (from[e] toblood)'
6186	Deoxyribose-Phosphate Aldolase'	56857	Exchange of Acetaldehyde (Excretion)'
6644	Cytochrome P450 17A1'	58421	Exchange of Acetaldehyde (SI)'
7035	Ethanolamine-Phosphate Phospho-Lyase (Deaminating)'	60934	Exchange of Acetaldehyde (Kidney)'
9045	"Aldehyde Dehydrogenase (Acetaldehyde, NAD)"'	69647	Exchange of Acetaldehyde (from[e] toblood)'
9100	Acetaldehyde Reversible Transport'	72324	Exchange of Acetaldehyde (GI)'
10618	Exchange of Acetaldehyde (from[e] toblood)'	76835	Acetaldehyde Mitochondrial DiffusionAcetaldehyde Reversible Transport, Endoplasmatic ReticulumAcetaldehyde Peroxisomal DiffusionAcetaldehyde Reversible Transport (BBB)'
10754	"Aldehyde Dehydrogenase (Acetaldehyde, NADP)"'	80719	Acetaldehyde Reversible Transport'
10905	Deoxyribose-Phosphate Aldolase'	80978	Acetaldehyde Reversible Transport'
11411	Ethanolamine-Phosphate Phospho-Lyase (Deaminating)'	81098	Pancreas_EX_acald[luP]'
11806	"Aldehyde Dehydrogenase (Acetaldehyde, NAD)"'		

7.2.4 Correlation between Drink Concentration and Gut Absorption

$$\mathbf{kStom} = \mathbf{0.7135} * \mathbf{Drink\%^2} - \mathbf{0.0985} * \mathbf{Drink\%} + \mathbf{0.0112} \quad \text{SI.31}$$

$$\mathbf{kStomSI} = \mathbf{1.953} * \mathbf{Drink\%^2} - \mathbf{0.168} * \mathbf{Drink\%} + \mathbf{0.0255} \quad \text{SI.32}$$

$$\mathbf{kSI} = \mathbf{-0.006} * \mathbf{Drink\%^2} - \mathbf{0.0686} * \mathbf{Drink\%} + \mathbf{0.0615} \quad \text{SI.33}$$

7.2.5 Effect of Tolerance on Model Smoothness

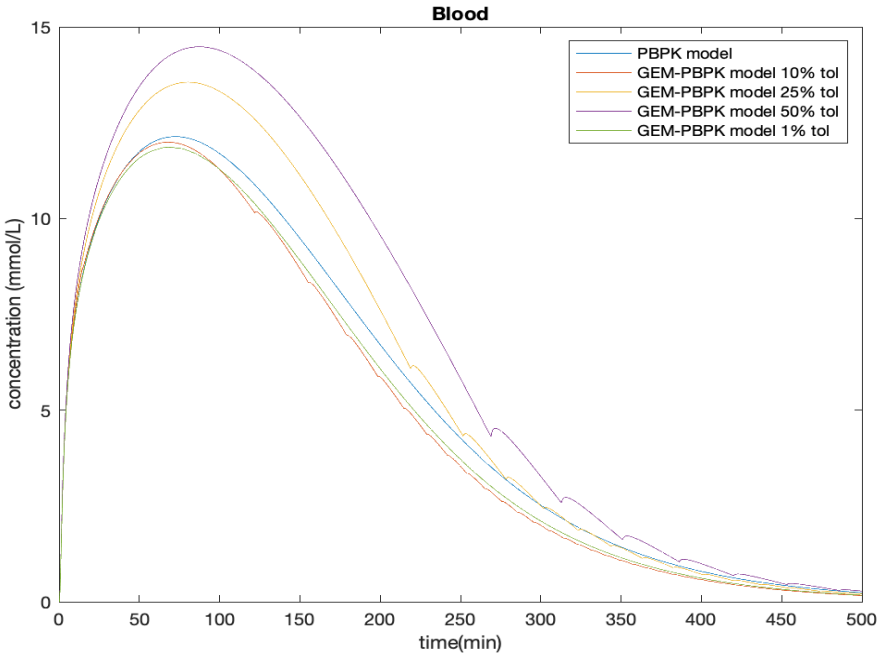

Fig SI.1 effect of tolerance on smoothness of model. As tolerance decreases, the curve better approximates the normal PBPK model. The predictions at 1% and 10% are at lower values when compared to the PBPK model because the GEM model also predicts for methods of ethanol elimination beyond Alcohol Dehydrogenase.

7.2.6 Liver Damage Simulation

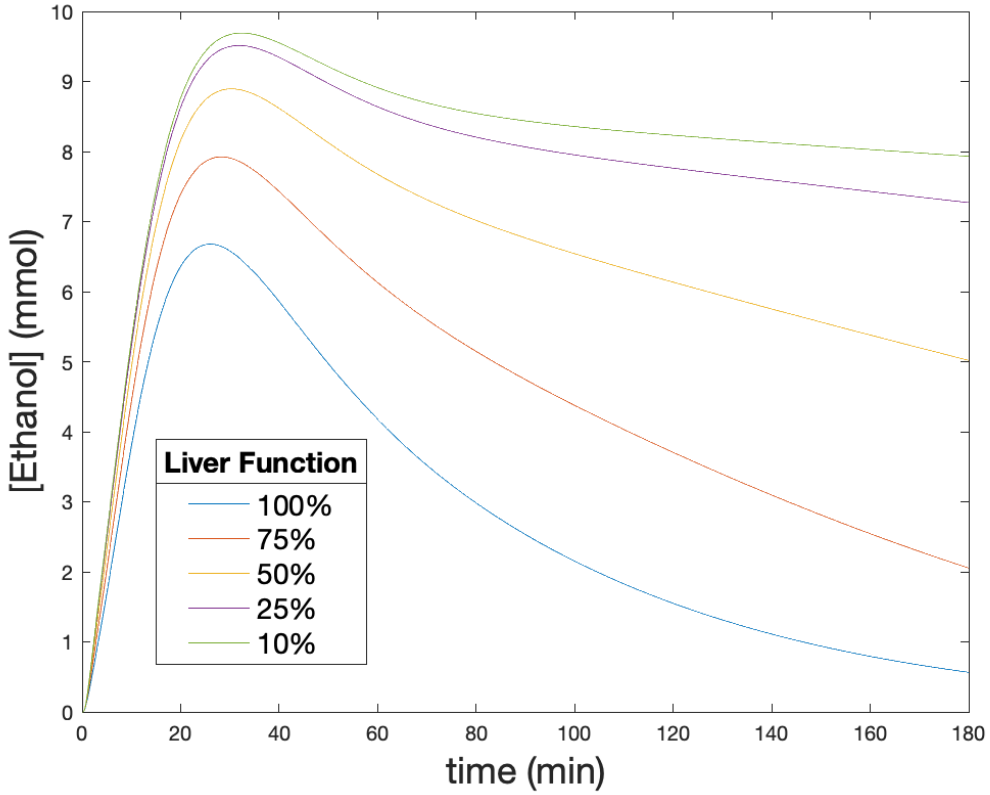

Fig. SI.2 Time-Concentration curves for ethanol metabolism with varying amounts of liver function. Simulations were performed with 20% ethanol for 25.6 year old men weighing 74.5kg with height = 180cm and 20% body fat drinking 0.25g/kg ethanol.

7.2.7 Correlation between Disulfiram concentration and ALDH2 activity

$$\mathbf{aALDH} = \mathbf{0.0015} * [\mathbf{Disulfiram}]^{\mathbf{2}} - \mathbf{0.0734} * [\mathbf{Disulfiram}] + \mathbf{1} \quad \text{SI.34}$$

Disulfiram concentration is in uM

7.2.8 Multi-Dose Curves

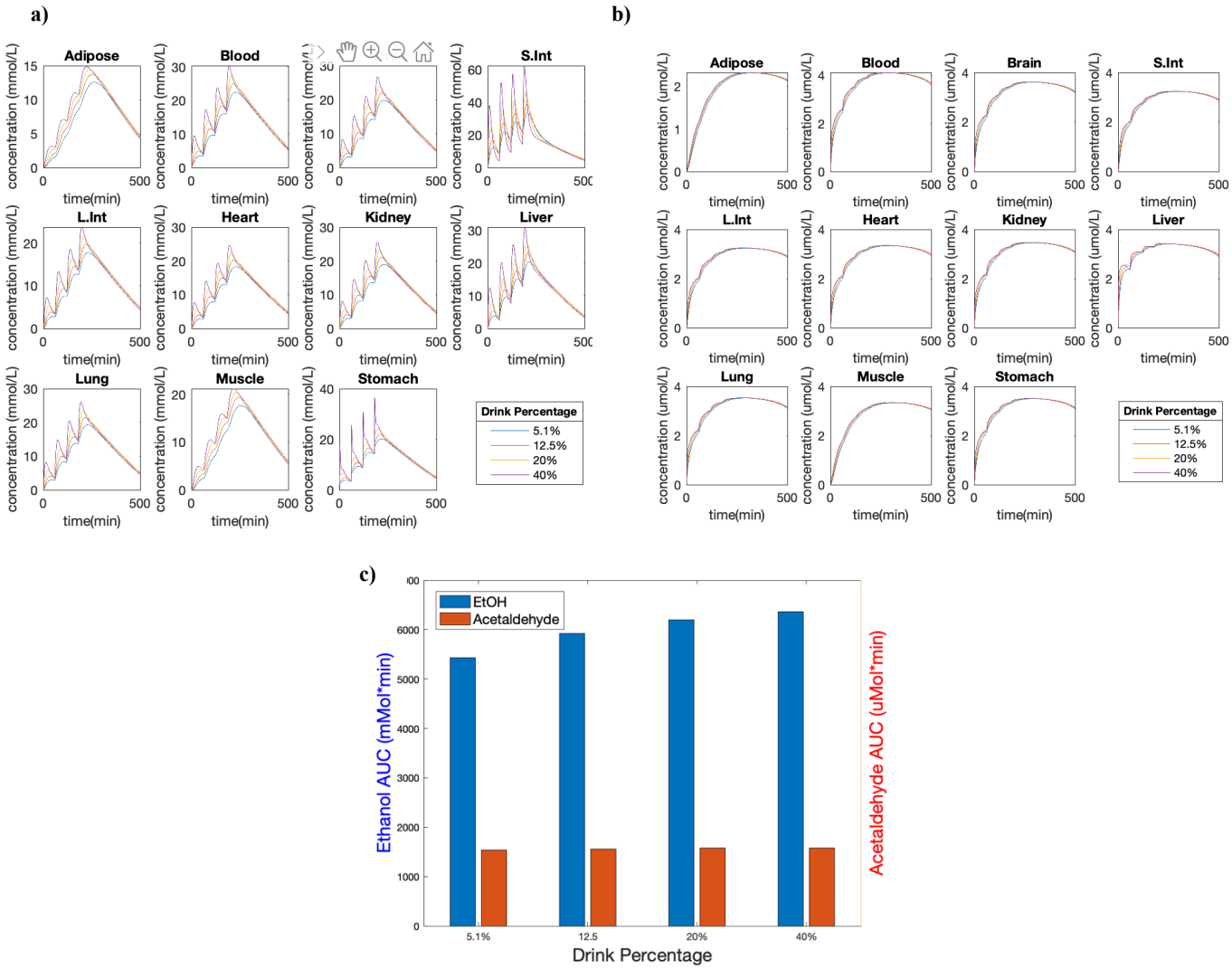

Fig. SI.3 Time-Concentration curves for ethanol metabolism with a dose every 120 minutes. Simulations were performed with 20% ethanol for 25.6 year old men weighing 74.5kg with height = 180cm and 20% body fat drinking 0.25g/kg ethanol. **(a)** Multi-dosing curves for ethanol concentration in various tissue compartments. **(b)** Multi-dosing curves for acetaldehyde concentration in various tissue compartments. **(c)** Area Under the Curve for both ethanol and acetaldehyde in the liver.